

Review

Recent advances in application of graphitic carbon nitride-based catalysts for degrading organic contaminants in water through advanced oxidation processes beyond photocatalysis: A critical review



Yang Yang^{a,b}, Xin Li^{a,b}, Chengyun Zhou^{a,b}, Weiping Xiong^{a,b}, Guangming Zeng^{a,b,*}, Danlian Huang^{a,b,*}, Chen Zhang^{a,b,*}, Wenjun Wang^{a,b}, Biao Song^{a,b}, Xiang Tang^{a,b}, Xiaopei Li^{a,b}, Hai Guo^{a,b}

^a College of Environmental Science and Engineering, Hunan University, Changsha 410082, PR China

^b Key Laboratory of Environmental Biology and Pollution Control, Hunan University, Ministry of Education, Changsha 410082, PR China

ARTICLE INFO

Article history:

Received 14 June 2020

Revised 16 July 2020

Accepted 17 July 2020

Available online 18 July 2020

Keywords:

Advanced oxidation processes
Carbon nitride
Organic pollutants
Degradation
Water treatment

ABSTRACT

Advanced oxidation processes (AOPs) have attracted much interest in the field of water treatment owing to their high removal efficiency for refractory organic contaminants. Graphitic carbon nitride ($\text{g-C}_3\text{N}_4$)-based catalysts with high performance and cost effectiveness are promising heterogeneous catalysts for AOPs. Most research on $\text{g-C}_3\text{N}_4$ -based catalysts focuses on photocatalytic oxidation, but increasingly researchers are paying attention to the application of $\text{g-C}_3\text{N}_4$ -based catalysts in other AOPs beyond photocatalysis. This review aims to concisely highlight recent state-of-the-art progress of $\text{g-C}_3\text{N}_4$ -based catalysts in AOPs beyond photocatalysis. Emphasis is made on the application of $\text{g-C}_3\text{N}_4$ -based catalysts in three classical AOPs including Fenton-based processes, catalytic ozonation and persulfates activation. The catalytic performance and involved mechanism of $\text{g-C}_3\text{N}_4$ -based catalysts in these AOPs are discussed in detail. Meanwhile, the effect of water chemistry including pH, water temperature, natural organic matter, inorganic anions and dissolved oxygen on the catalytic performance of $\text{g-C}_3\text{N}_4$ -based catalysts are summarized. Moreover, the reusability, stability and toxicity of $\text{g-C}_3\text{N}_4$ -based catalysts in water treatment are also mentioned. Lastly, perspectives on the major challenges and opportunities of $\text{g-C}_3\text{N}_4$ -based catalysts in these AOPs are proposed for better developments in the future research.

© 2020 Elsevier Ltd. All rights reserved.

1. Introduction

With fast growth of industrialization and population, the water contamination caused by organic pollutants is becoming a serious global issue that threatens public health and safety (Li et al., 2020b; Yang et al., 2020b, 2018a). Various synthetic organics (e.g. dyes, pesticides, pharmaceuticals and personal care products (PPCPs), etc.) are discharged into wastewaters and eventually enter natural water bodies (Chen et al., 2020b; Lefebvre and Malletta, 2006; Liu and Wong, 2013; Tian et al., 2020). It is well known that most of these compounds are persistent organic pollutants (POPs), which will threaten the living organisms, including human beings (Brown and Wright, 2016; Muir and Howard, 2006; Song et al., 2018). A variety of physical and biological treatment

methods have been employed for the removal of organic pollutants from water, such as adsorption, ultrafiltration and coagulation (Lei et al., 2020a; Xiong et al., 2019; Zhang et al., 2016). However, insufficient capacity to remove trace organic pollutants and possible secondary pollution limit their practical applications. Thus, highly efficient and environmentally friendly treatment processes are required for the removal of residual organic pollutants from water.

Advanced oxidation processes (AOPs) have stimulated great interest from researchers around the world owing to their high efficiency in degrading and even mineralizing organic pollutants from water (Jia et al., 2020; Klavarioti et al., 2009; Tan et al., 2020; Yang et al., 2020c). Moreover, AOPs are more environmentally friendly than physical and biological treatment processes as they will not release masses of deleterious residues or divert organic pollutants from one phase to another (Oturan and Aaron, 2014; Ye et al., 2019a; Yi et al., 2019). In AOPs, almost all types of organic pollutants can be degraded or mineralized into intermediate products or CO_2 and H_2O . The outstanding activity and versatility of

* Corresponding authors at: College of Environmental Science and Engineering, Hunan University, Changsha 410082, PR China.

E-mail addresses: zgming@hnu.edu.cn (G. Zeng), huangdanlian@hnu.edu.cn (D. Huang), zhangchen@hnu.edu.cn (C. Zhang).

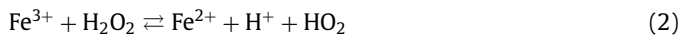
AOPs are originated from the production of highly reactive species such as $\bullet\text{OH}$, $\text{SO}_4^{\bullet-}$, ${}^1\text{O}_2$ and $\bullet\text{O}_2^-$, which can efficiently attack the target contaminants leading to their decomposition (Li et al., 2020c; Wang and Xu, 2012; Yang et al., 2018b). Specifically, AOPs include homogeneous AOPs and heterogeneous AOPs. The heterogeneous AOPs generally utilize solid catalysts in combination with other systems (H_2O_2 , O_3 , persulfates, light, etc.) to degrade organic pollutants (Lin et al., 2020; Liu et al., 2019; Yuan et al., 2020). Compared with homogeneous catalysts, the main advantage of heterogeneous catalysts is the convenience of catalysts recovery. For practical applications in water decontamination, heterogeneous catalysts must meet some requirements, such as high activity, sustainability as well as physical and chemical stability. Accordingly, many efforts have been paid to the exploitation of efficient and durable heterogeneous catalysts for AOPs.

Graphitic carbon nitride ($\text{g-C}_3\text{N}_4$) has recently emerged as promising catalyst in AOPs because of its simple synthesis, low cost and toxicity, unique electronic structure and good stability (He et al., 2019b; Wang et al., 2020c; Zhou et al., 2019). As a metal-free conjugated polymer semiconductor, the relatively narrow bandgap (about 2.7 eV) of $\text{g-C}_3\text{N}_4$ endows it with a superior light absorption capacity (Yang et al., 2019d; Zhou et al., 2020a). Besides, the inherent functional groups and vacancies as well as the sp^2 hybridized carbon network are conductive to the generation and migration of delocalized electrons (Wang et al., 2018; Yang et al., 2020a). Meanwhile, $\text{g-C}_3\text{N}_4$ possesses a two-dimensional layered structure and six nitrogen lone-pair electrons, which are in favor of the immobilization and dispersion of metal species (Song et al., 2019a; Yang et al., 2019c). Benefiting from these excellent characteristics, $\text{g-C}_3\text{N}_4$ -based catalysts have been widely applied in AOPs, especially photocatalysis, to degrade organic pollutants from water (Guo et al., 2020a; Wang et al., 2019d, 2020e; Zhang et al., 2020a). And considerable reviews present broad introduction on the application of $\text{g-C}_3\text{N}_4$ -based catalysts in photocatalytic oxidation (Ding et al., 2017; Hao et al., 2020; Huang et al., 2019a; Mamba and Mishra, 2016; Ong et al., 2016). However, it is hard to achieve deep mineralization for organic pollutants using photocatalysis. Moreover, the changeable weather and complex photoreactor also restrict the extensive, large-scale and practical applications of photocatalysis (Loeb et al., 2019; Melchionna and Fornasiero, 2020; Wang et al., 2020a). In recent years, some other AOPs based on $\text{g-C}_3\text{N}_4$ -based catalysts have drawn great attention owing to their superior oxidation ability and operational stability, such as Fenton-based processes, catalytic ozonation and persulfates activation. In these processes, oxidants like H_2O_2 , O_3 and persulfates can be activated by $\text{g-C}_3\text{N}_4$ -based catalysts to generate highly reactive species for the degradation of organic contaminants in water (Fig. 1). Therefore, it is necessary to give a timely review of the progress of $\text{g-C}_3\text{N}_4$ -based catalysts in those concerned AOPs.

As a state-of-the-art review, the chief objective of this work is to highlight recent advances of $\text{g-C}_3\text{N}_4$ -based catalysts in AOPs beyond photocatalysis. The catalytic performance and reaction mechanism of $\text{g-C}_3\text{N}_4$ -based catalysts in three classical AOPs including Fenton-based processes, catalytic ozonation and persulfates activation are discussed. Meanwhile, the effect of water chemistry on the catalytic performance of $\text{g-C}_3\text{N}_4$ -based catalysts are summarized, such as pH, water temperature, natural organic matter, inorganic anions and dissolved oxygen. Additionally, the reusability, stability and toxicity of $\text{g-C}_3\text{N}_4$ -based catalysts in water treatment are mentioned. Ultimately, the challenges and opportunities faced by $\text{g-C}_3\text{N}_4$ -based catalysts in these AOPs are presented.

2. Application of $\text{g-C}_3\text{N}_4$ -based catalysts in Fenton-based processes

Fenton reaction is recognized as one of the most effective strategy for degrading organic contaminants from water (Deng et al., 2020; Li et al., 2020a; Pignatello et al., 2006). In a typical Fenton reaction, Fe^{2+} catalyzes the decomposition of H_2O_2 to generate $\bullet\text{OH}$ (Eq. (1)) (Khataee et al., 2016). The generated $\bullet\text{OH}$ can quickly destroy the pollutant structure owing to its high oxidation potential. More importantly, the formed Fe^{3+} can be reduced to Fe^{2+} by H_2O_2 through the Fenton-like reaction (Eq. (2)) (Gholami et al., 2020b), which enables the continuous generation of $\bullet\text{OH}$. However, the application of conventional Fenton reaction is generally restricted by its inherent shortcomings such as narrow range of working pH, accumulation of Fe-containing sludge and poor reusability. To overcome these problems, numerous heterogeneous Fenton-like catalysts were developed to replace the homogeneous process (Cheng et al., 2018b; Huang et al., 2019b; Li et al., 2019c).



In the past few years, introducing metal species into $\text{g-C}_3\text{N}_4$ to construct Fenton-like catalysts for the degradation of organic pollutants in water (Table 1) has attracted great interest because of its excellent characteristics such as efficient catalytic activity, high stability and environmental friendliness. For example, Wang and Nan (2020) utilized Fe-doped $\text{g-C}_3\text{N}_4$ ($\text{Fe-g-C}_3\text{N}_4$) to catalyze the decomposition of H_2O_2 for degrading methylene blue (MB). The pyridinic N in $\text{g-C}_3\text{N}_4$ was easily bonded with the Fe atoms to form active sites, thus enhancing the catalytic activity. Owing to the presence of abundant active sites of Fe(II)-N_x and Fe(III)-N_x , the $\text{Fe-g-C}_3\text{N}_4$ exhibited excellent activity in Fenton-like oxidation, achieving 83.7% removal of total organic carbon (TOC) in 60 min. Moreover, the $\text{g-C}_3\text{N}_4$ supported iron oxide (CN@IO) was also reported to be an efficient Fenton-like catalyst for the degradation of ciprofloxacin (CIP) (Ding et al., 2019). Under the experimental conditions, almost all CIP was degraded and 48.5% CIP was mineralized, which was ascribed to the accelerated redox cycle of Fe(III)/Fe(II) by $\text{g-C}_3\text{N}_4$. Apart from iron species, some other metal species have also been introduced into $\text{g-C}_3\text{N}_4$ to fabricate Fenton-like catalyst. The Cu(I) was incorporated into $\text{g-C}_3\text{N}_4$ for the degradation of various organic pollutants (Ma et al., 2019b). During the formation of $\text{g-C}_3\text{N}_4$, the Cu(II) could be reduced by the released carbon and nitride fragments to form Cu(I) , which would be conductive to the enhancement of Fenton-like activity. The removal efficiencies of Rhodamine B (RhB), Acid Red 73 (AR 73), bisphenol A (BPA) and tetracycline (TC) were 99.2%, 96.0%, 94.6% and 84.4%, respectively, indicating that the Cu(I) -doped $\text{g-C}_3\text{N}_4$ ($\text{Cu(I)-g-C}_3\text{N}_4$) was an effective Fenton-like catalyst to degrade different kinds of organic pollutants. In addition, Ge et al. (2018) combined the MgO with $\text{g-C}_3\text{N}_4$ to activate H_2O_2 for the degradation of organic dyes. The $\text{g-C}_3\text{N}_4/\text{MgO}$ presented outstanding degradation activities for both anionic and cationic dyes, such as methyl orange (MO), MB and RhB. It was found that the Mg–N and C–O bonding between MgO and $\text{g-C}_3\text{N}_4$ played a critical role in the degradation reaction via activating H_2O_2 to generate $\bullet\text{OH}$.

Nevertheless, the content of metals in these $\text{g-C}_3\text{N}_4$ -based catalysts was relatively low, resulting in the unsatisfactory catalytic performance in Fenton-like oxidation (Bicalho et al., 2017; Luo et al., 2016). And when the metal content increased, it eas-

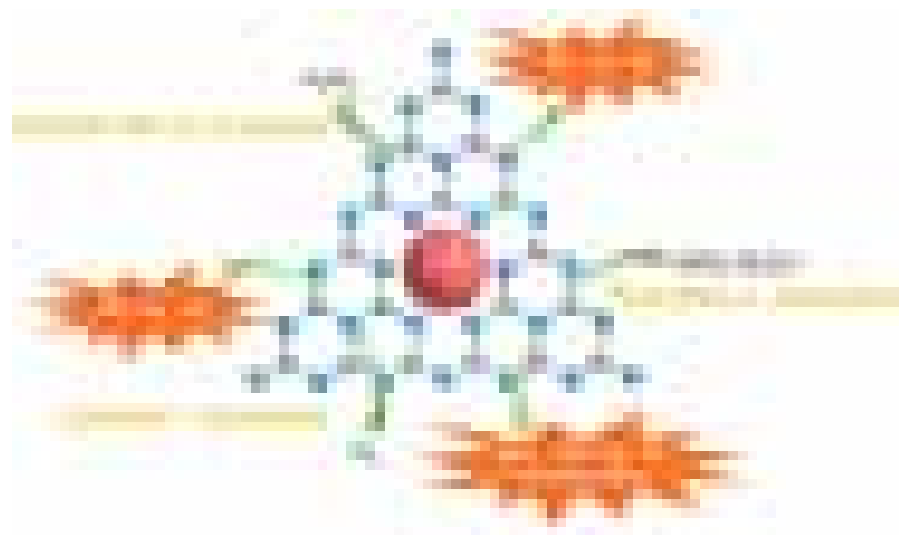


Fig. 1. The catalytic mechanisms of $\text{g-C}_3\text{N}_4$ -based catalysts for organic contaminants degradation.

Table 1.

Catalytic activity of $\text{g-C}_3\text{N}_4$ -based catalysts in Fenton-based processes.

Catalyst	Reaction conditions				Catalytic efficiency			Key reactive species	Reference
	Pollutant[P]	[C]	[H ₂ O ₂]	pH	DE (min)	k_{obs} (min ⁻¹)	TOC (min)		
Fe-g-C ₃ N ₄	MB	100 mg L ⁻¹	0.2 g L ⁻¹	199.4 mM	7.21	100% (60)	0.0886	52.5% (60)	•OH, •O ₂ ⁻
CN@IO	CIP	20 mg L ⁻¹	1.0 g L ⁻¹	5.6 mM	3	100% (60)	–	48.5% (120)	•OH
Fe-g-C ₃ N ₄ /GMC	AR 73	50 mg L ⁻¹	0.8 g L ⁻¹	40 mM	–	99.2% (40)	0.1837	42.9% (40)	•OH
Cu-g-C ₃ N ₄	RhB	10 mg L ⁻¹	0.2 g L ⁻¹	300 mM	neutral	92.3% (15)	–	42% (60)	•OH, •O ₂ ⁻ , ¹ O ₂
Cu(I)-g-C ₃ N ₄	RhB	50 mg L ⁻¹	0.8 g L ⁻¹	40 mM	neutral	99.2% (60)	–	22.8% (60)	•O ₂ , •OH
CuFe ₂ O ₄ -MCN	4-CP	100 mg L ⁻¹	1.0 g L ⁻¹	2 g L ⁻¹	4	100% (60)	0.076	59% (60)	•OH
Cu-Al ₂ O ₃ -g-C ₃ N ₄	BPA	20 mg L ⁻¹	0.5 g L ⁻¹	12.5 mM	7	97.3% (30)	–	72.3% (120)	•OH
OH-CCN/CuCo-Al ₂ O ₃	BPA	0.1 mM	0.8 g L ⁻¹	10 mM	7	96.3% (30)	0.11	67.1% (30)	•OH
CN-Cu(II)-CuAlO ₂	BPA	25 mg L ⁻¹	1.0 g L ⁻¹	10 mM	6–7	95.5% (120)	0.027	41.5% (180)	•OH

[P]: pollutant concentration; [C]: catalyst dosage; [H₂O₂]: H₂O₂ concentration; DE: degradation efficiency; k_{obs} : apparent rate constant; TOC: total organic carbon; MB: methylene blue; CIP: ciprofloxacin; AR 73: Acid Red 73; RhB: Rhodamine B; 4-CP: 4-chlorophenol; BPA: bisphenol A.

ily aggregated to form large particles, leading to a reduction in the number of catalytic active sites (Teixeira et al., 2018). To effectively improve the activity of $\text{g-C}_3\text{N}_4$ -based catalysts in Fenton-like oxidation, some $\text{g-C}_3\text{N}_4$ -based catalysts with high metal content and dispersion were developed. For example, Zhu et al. (2019) synthesized Cu-doped $\text{g-C}_3\text{N}_4$ (Cu-g-C₃N₄) with high content of Cu-N_x species by calcining the precursor of melamine templated crystalline copper chloride. In the optimal Cu-g-C₃N₄ composite, the Cu content was up to 25.9 wt% and the Cu was uniformly dispersed in the $\text{g-C}_3\text{N}_4$ matrix. The presence of abundant Cu-N_x species could accelerate the decomposition of H₂O₂ to form •OH. Therefore, the Cu-g-C₃N₄ presented superior catalytic activities for the degradation of RhB, MO and MB. Moreover, decorating $\text{g-C}_3\text{N}_4$ with metals in forms of ultra-small clusters and single-atoms has drawn much attention due to the high atom-utilization efficiency (Li et al., 2019e). An et al. (2018) successfully embedded high-density ultra-small Fe clusters and single-atom Fe sites in $\text{g-C}_3\text{N}_4$ (I-FeN_x/g-C₃N₄) by calcining a mixture of Fe-imidazole coordination compound and melamine. The “nitrogen pots” with six nitrogen lone-pair electrons in $\text{g-C}_3\text{N}_4$ could efficiently trap and stabilize ultra-small Fe clusters and single-atom Fe sites. As shown in Fig. 2a-d, high-density (18.2 wt%) ultra-small Fe clusters and single-atom Fe sites were uniformly dispersed in the $\text{g-C}_3\text{N}_4$ and no iron nanoparticles could be observed. The energy dispersive X-ray spectroscopy images also showed the uniform distribution of C, N and Fe elements (Fig. 2e). The X-ray absorption near-edge structure (XANES) spectra (Fig. 2f) and extended X-ray absorption fine structure (EXAFS) spectra (Fig. 2g) further demonstrated that

the Fe-N_x structure was formed. As the Fe(II)-N_x active sites could quickly decompose H₂O₂ to produce •OH, the I-FeN_x/g-C₃N₄ catalyst exhibited excellent removal efficiency for MB despite no light (Fig. 2h). Additionally, the iron leaching of I-FeN_x/g-C₃N₄ catalyst was 0.69 mg L⁻¹, which was much lower than the nano-Fe₃O₄ (2.3 mg L⁻¹) and Fe₃O₄ (9.8 mg L⁻¹) as well as the European Union standard (2 mg L⁻¹) (Khataee et al., 2017; Li et al., 2019b; Xu and Wang, 2012), indicating that the Fe(II)-N_x configurations was stably implanted into $\text{g-C}_3\text{N}_4$.

Although some achievements have been done on these $\text{g-C}_3\text{N}_4$ -based Fenton-like catalysts, there are still some inadequacies and need further improvements. Typically, the reduction of the metals anchored on $\text{g-C}_3\text{N}_4$ through the oxidation of H₂O₂ is slow, leading to the insufficient redox cycle of the metals. Additionally, in this process, H₂O₂ is finally decomposed into O₂ or •O₂⁻, which will cause the waste of H₂O₂ (Bokare and Choi, 2014; Lyu et al., 2015). To resolve these problems, the $\text{g-C}_3\text{N}_4$ -based catalysts with dual reaction centers were developed to enhance the catalytic activity in Fenton-like process. For example, Xu et al. (2018) constructed a novel Cu-Al₂O₃-g-C₃N₄ catalyst to promote the selective conversion of H₂O₂ to •OH for enhancing the Fenton-like catalytic activity. In the Cu-Al₂O₃-g-C₃N₄ system, the electron-rich area around Cu was formed because of the higher electronegativity of Cu than Al as well as the Cu-π interactions between Cu and $\text{g-C}_3\text{N}_4$. Therefore, the •OH could be generated by two different electron transfer processes: the one was from the electron-rich Cu center to H₂O₂ to produce •OH, and the other was from H₂O to the electron-poor site to form •OH. Benefiting from the significant increase of •OH gen-

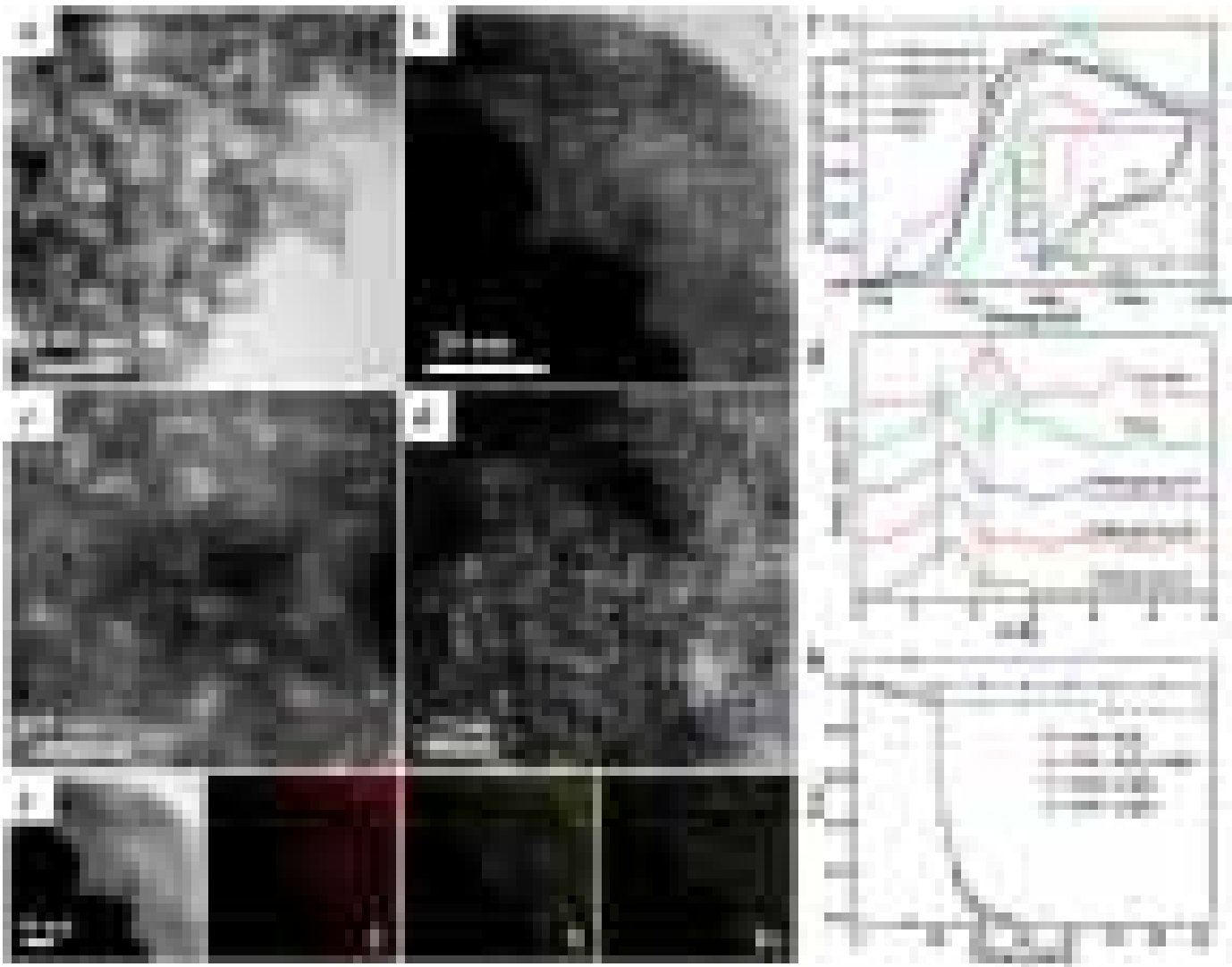


Fig. 2. (a) TEM image, (b-d) HAADF-STEM images and (e) the corresponding element mappings for the C, N, and Fe atoms of I- $\text{FeN}_x/\text{g-C}_3\text{N}_4$ -5 catalyst. (f) K-edge XANES spectra and (g) R-space EXAFS magnitudes of different samples. (h) Removal efficiency of MB using I- $\text{FeN}_x/\text{g-C}_3\text{N}_4$ -5 under various conditions. Reproduced with permission from Ref. (An et al., 2018). Copyright 2018 American Chemical Society.

eration, the Cu-Al₂O₃-g-C₃N₄ catalyst exhibited high activities for the degradation of organic pollutants including RhB, BPA, MB, 2,4-dichlorophenoxyacetic acid (2,4-D) and phenytoin sodium (PHT).

Besides, Lyu et al. (2018) combined g-C₃N₄ with in situ formed Cu(II) on the surface of CuAlO₂ substrate to fabricate a new Fenton-like catalyst. The C–O–Cu bonding bridge on g-C₃N₄-Cu(II)-CuAlO₂ could efficiently strengthen the cation- π interaction through the charge transfer. As verified by the density functional theory (DFT) calculations (Fig. 3a and b) and electron paramagnetic resonance (EPR) analysis (Fig. 3c), the dual reaction centers were formed around the Cu and C sites in CN-Cu(II)-CuAlO₂, which was ascribed to the cation- π interaction via the C–O–Cu linkage. As depicted in Fig. 3d, the H₂O₂ was efficiently reduced by electrons to •OH on the electron-rich Cu center. Meanwhile, the electrons on H₂O₂ and pollutants were trapped by the electron-poor C center and then diverted to the electron-rich area through the C–O–Cu linkage. Therefore, the catalytic activity of CN-Cu(II)-CuAlO₂ for the degradation of BPA was greatly enhanced compared with that of g-C₃N₄ and CuAlO₂. Moreover, the CN-Cu(II)-CuAlO₂ also exhibited excellent catalytic activities for the degradation of other refractory pollutants, such as phenol, 2-chlorophenol, ibuprofen and phenytoin, indicating its huge potential in water purification.

To further improve the activity of g-C₃N₄-based catalysts in Fenton-like oxidation, carbonaceous materials with excellent electron transport property and chemical stability were introduced (Ma et al., 2019a; Wang et al., 2019a). For example, the graphitized mesoporous carbon (GMC) was hybridized with Fe-g-C₃N₄ for the degradation of AR 73 (Ma et al., 2017). The GMC not only provided a mesoporous structure for the growth of g-C₃N₄, but also offered a similar sp² bonding structure to promote the electron transfer. Benefiting from the accelerated Fe(III)/Fe(II) redox cycle, the Fe-g-C₃N₄/GMC composite showed high activity for AR 73 degradation in the Fenton-like reaction, obtaining 99.2% removal in 40 min. Additionally, enhanced adsorption (10.7%) caused by the introduction of GMC in Fe-g-C₃N₄/GMC composite might also contribute to the accelerated degradation of AR 73. The carbon nanodots (CDs) were also effective in enhancing the catalytic activity of Fe(II)-doped g-C₃N₄ (Fe(II)-g-C₃N₄) in Fenton-like reaction because they could promote the decomposition of H₂O₂ to produce more •OH (Fang et al., 2019). In the presence of H₂O₂, the CDs/Fe(II)-g-C₃N₄ composite presented superior activity in the Fenton-like system for MB degradation. Quenching experiments and EPR measurements suggested that •OH and •O₂⁻ were the main reactive species re-

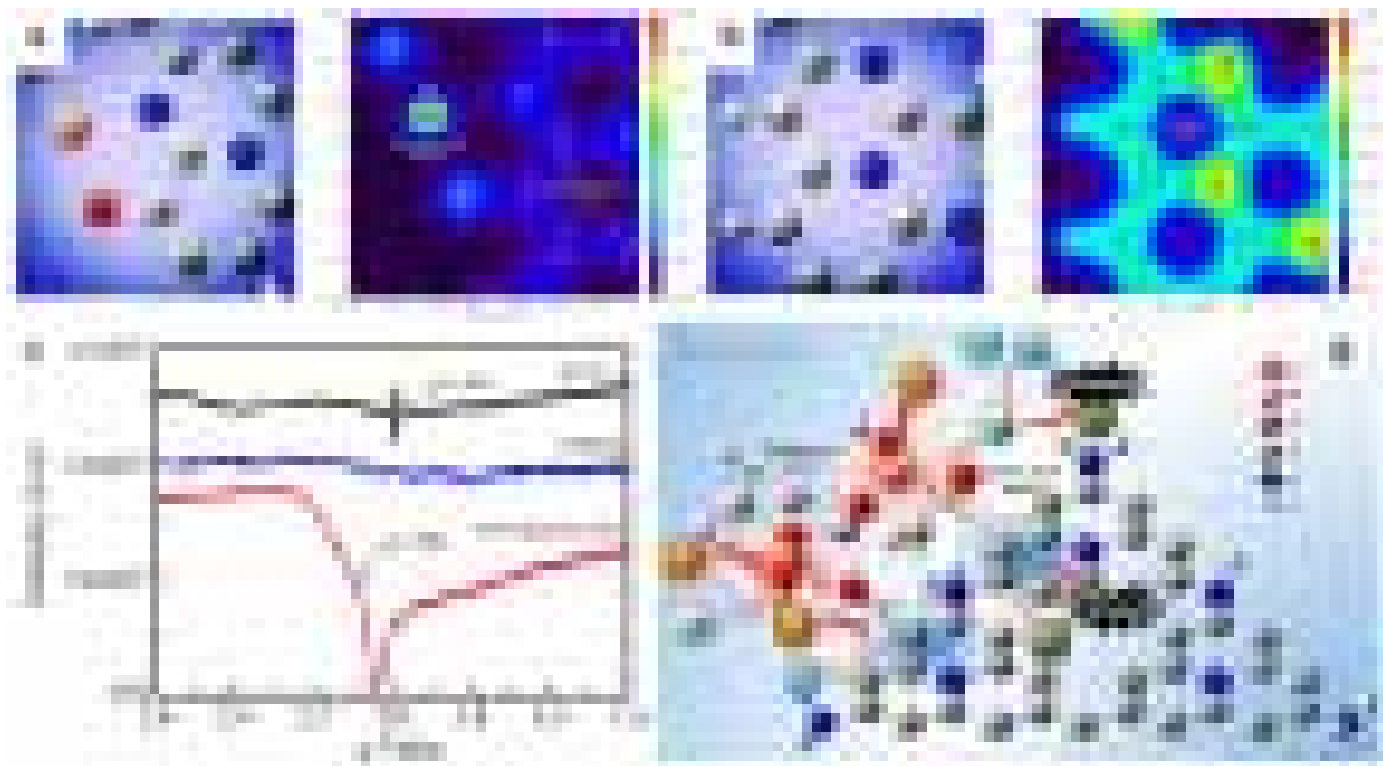


Fig. 3. DFT calculations for the optimized structure and the corresponding two-dimensional valence-electron density color-filled maps of the CN-Cu(II)-CuAlO₂ model in (a) -Cu(II)-CN vision fragment and (b) -CN vision fragment. (c) EPR spectra of different samples. (d) Fenton-like oxidation mechanism on CN-Cu(II)-CuAlO₂. Reproduced with permission from Ref. (Lyu et al., 2018). Copyright 2018 American Chemical Society.

sponsible for the MB degradation, and •O₂⁻ was originated from the reaction between H₂O₂ and •OH.

The utilization of solar light to construct a photo-Fenton system is also an effective way to enhance the performance of g-C₃N₄-based catalysts as g-C₃N₄-based catalysts can be easily excited by visible light to generate electrons and holes (Li et al., 2016). In this process, the Fe(III)/Fe(II) redox cycle can be greatly accelerated by the photogenerated electrons, thereby facilitating the decomposition of H₂O₂ to •OH and promoting the degradation of organic pollutants (Herney-Ramirez et al., 2010; Soon and Hameed, 2011). For example, a Fe₂O₃ quantum dots (QDs)/g-C₃N₄ composite was fabricated to catalyze the decomposition of H₂O₂ for degrading *p*-nitrophenol under visible light (Xi et al., 2019). The excellent separation and transfer of photogenerated charges on Fe₂O₃ QDs/g-C₃N₄ could result in the continuous and fast conversion of Fe(III)/Fe(II). Therefore, the activation of H₂O₂ was improved and the degradation rate of *p*-nitrophenol was dramatically enhanced. Moreover, a photo-Fenton-like membrane was assembled for wastewater treatment by using g-C₃N₄ sol and Fe-containing polyoxometalates (Fe-POMs) as precursors (Lan et al., 2019). Owing to the synergistic effect of photocatalysis and Fenton-like reaction, the photo-Fenton-like membrane displayed outstanding self-catalytic capacity for degrading retained pollutants. Besides, the construction of photo-electro-Fenton-like system based on g-C₃N₄ has also stimulated great research interest (Yue et al., 2018). In this process, the H₂O₂ is in situ generated in the cathode through the two-electron reduction of O₂, and then the H₂O₂ can be activated by the g-C₃N₄-based catalysts to generate •OH for the degradation of organic pollutants. Recently, a photo-electro-Fenton-like system with WO₃/g-C₃N₄ was fabricated for CIP degradation (Bai et al., 2019). Compared with the photocatalysis system and electro-Fenton-like system, the photo-electro-Fenton-like sys-

tem showed superior degradation efficiency for CIP and achieved 80.3% mineralization efficiency within 120 min.

In a word, in Fenton-based processes, g-C₃N₄ can act as an excellent support to immobilize metal species, thus improving the catalytic activity and stability of g-C₃N₄-based catalysts. Specifically, the layered structure of g-C₃N₄ is an effective support for loading of the metal species, which can suppress the mobility, improve the dispersion and avoid the aggregation of metal species. Meanwhile, the “nitrogen pots” with six nitrogen lone-pair electrons in g-C₃N₄ are ideal sites for trapping metal species. The general catalytic mechanisms of g-C₃N₄-based catalysts during Fenton-based processes are depicted in Fig. 1. The active metal species on g-C₃N₄-based catalysts can decompose H₂O₂ to generate •OH, •O₂⁻ and ¹O₂, which will lead to the degradation of organic pollutants.

3. Application of g-C₃N₄-based catalysts in catalytic ozonation

As a powerful oxidant, it is well known that O₃ can react with many organic pollutants. However, the oxidation of some organic pollutants by O₃ is relatively slow because of the selectivity of O₃ to organics, leading to the incomplete removal of pollutants or formation of toxic intermediate products (Esplugas et al., 2007; Hubner et al., 2015). In addition, O₃ presents a low mineralization rate for organic pollutants due to the generation and accumulation of some intermediate products that cannot react with O₃, such as aldehydes and carboxylic acids (Nawrocki and Kasprzykhordern, 2010). To address these issues, some advanced technologies such as O₃/H₂O₂ process and O₃/UV process were developed to activate O₃ (Miklos et al., 2018). Among these, the catalytic ozonation process has stimulated much research interest as it can promote the activation of O₃ to generate reactive oxygen species (ROS) by the addition of some catalysts

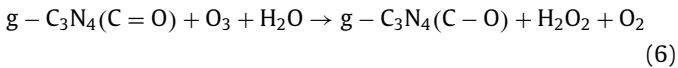
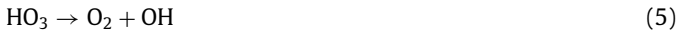
Table 2Catalytic activity of g-C₃N₄-based catalysts in catalytic ozonation.

Catalyst	Pollutant	[P]	[C]	[O ₃]	pH	Reaction conditions	Catalytic efficiency	k _{obs} (min ⁻¹)	TOC (min)	Key reactive species	Reference
g-C ₃ N ₄	p-CBA	0.084 mM	0.5 g L ⁻¹	2 mg L ⁻¹	4.75	6.01	98% (30) 100% (30)	0.116 0.156	60% (30) 64% (30)	•OH, •O ₂ ⁻	(Song et al., 2019b)
O@g-C ₃ N ₄	ATZ	2 mg L ⁻¹	0.5 g L ⁻¹	5 mg min ⁻¹	6		92.91% (5)	0.6279	77.95% (15)	•O ₂ ⁻ , •OH	(Yuan et al., 2019)
Ce(III)-g-C ₃ N ₄	OA	0.5 mM	0.1 g L ⁻¹	6.6 mg min ⁻¹	3.5		96.1% (30)	-	90% (30)	•OH	(Xie et al., 2020)
ZVZ-g-C ₃ N ₄	ATZ	2 mg L ⁻¹	0.5 g L ⁻¹	5 mg min ⁻¹	6		96.5% (1.5)	1.852	-	•O ₂ ⁻ , •OH, ¹ O ₂	(Yuan et al., 2018b)
CuO/g-C ₃ N ₄	OA	50 mg L ⁻¹	0.5 g L ⁻¹	5 mg min ⁻¹	6		91% (15)	0.1349	73% (30)	•O ₂ ⁻ , •OH	(Liu et al., 2020a)
ZnO/g-C ₃ N ₄	ATZ	2 mg L ⁻¹	0.5 g L ⁻¹	5 mg min ⁻¹	6.5		99.5% (2)	2.73	76.8% (15)	•O ₂ ⁻ , •OH, ¹ O ₂	(Yuan et al., 2018a)
LaCoO ₃ /g-C ₃ N ₄	BZA	0.084 mM	0.25 g L ⁻¹	1 mg L ⁻¹	6.4		90% (30)	0.095	65% (120)	•OH, ¹ O ₂ , •O ₂ ⁻	(Zhang et al., 2019b)

[P]: pollutant concentration; [C]: catalyst dosage; [O₃]: O₃ concentration; DE: degradation efficiency; k_{obs}: apparent rate constant; TOC: total organic carbon; p-CBA: 4-chlorobenzoic acid; BZA: benzotriazole; ATZ: atrazine; OA: oxalic acid.

(Wang and Bai, 2017; Wang and Chen, 2020). Compared with homogeneous catalytic ozonation, heterogeneous catalytic ozonation is greener, more economical and more convenient. Therefore, many efforts have been devoted to developing novel heterogeneous catalysts for catalytic ozonation.

Graphitic carbon nitride-based catalysts have been demonstrated to be effective heterogeneous catalysts in catalytic ozonation for degrading organic pollutants from water Table 2). Normally, the delocalized electrons and surface oxygen-containing functional groups are responsible for the activity of g-C₃N₄ in catalytic ozonation. Song et al. (2019b) found that the g-C₃N₄ exhibited activity in catalytic ozonation for the degradation of 4-chlorobenzoic acid (p-CBA) and benzotriazole (BZA) due to the presence of electron-rich nitrogen vacancies and surface oxygen-containing functional groups (such as hydroxyl group and carbonyl group). Compared with the sole ozonation (apparent rate constant (k_{obs}): 0.069 and 0.057 min⁻¹), the catalytic ozonation by adding g-C₃N₄-Urea presented better activity for p-CBA and BZA degradation (k_{obs}: 0.116 and 0.156 min⁻¹). During the reaction, the O₃ captured the delocalized electrons from the electron-rich nitrogen vacancies in g-C₃N₄ to form the •O₃⁻ (Eq. (3)) and then the HO₃• (Eq. (4)), which rapidly transformed into •OH (Eq. (5)). Moreover, the O₃ decomposed aromatic rings in organic species to olefins, which subsequently reacted with O₃ to form H₂O₂. Meanwhile, the carbonyl group in g-C₃N₄ also enhanced the H₂O₂ production (Eq. (6)). And the reaction of H₂O₂ and O₃ could generate more •OH and •O₂⁻ (Eqs. (7) and (8)). Therefore, the activity of g-C₃N₄ in catalytic ozonation was greatly enhanced. In addition, the doping of O atoms could increase the amount of surface oxygen-containing functional groups and nitrogen vacancies of g-C₃N₄, thus enhancing the performance catalytic ozonation (Yuan et al., 2019). The degradation efficiency of atrazine (ATZ) through catalytic ozonation over the oxygen functionalized g-C₃N₄ (O@g-C₃N₄) was increased by 29.76% in comparison with the sole ozonation.



It has been reported that metal species could significantly promote the decomposition of O₃ to produce ROS (Wang and Bai, 2017; Wang et al., 2019b). Accordingly, numerous g-C₃N₄-based metal-containing catalysts have been constructed recently to realize the synergistic effect of g-C₃N₄ and metal species for efficient catalytic ozonation. For example, the ZnO/g-C₃N₄ was found to be highly active in catalytic ozonation and the k_{obs} of ATZ degradation was 2.73 min⁻¹, which was almost 10.5 times higher than that of ozone alone (Yuan et al., 2018a). The enhanced activity was owing to the host-guest interaction between g-C₃N₄ and ZnO, as well as the increased surface area and improved electron transfer ability. Tert-butanol (TBA), p-benzoquinone (p-BQ) and NaN₃ were utilized as ROS scavengers for •OH, •O₂⁻ and ¹O₂, respectively. The degradation efficiency of ATZ in ZnO/g-C₃N₄/O₃ system was greatly inhibited after the addition of ROS scavengers, implying that •O₂⁻, ¹O₂ and •OH were the major reactive species responsible for ATZ degradation. Besides, the g-C₃N₄ could also provide an ideal site to accommodate Ce(III), thus accelerating the formation of surface hydroxyl groups (Xie et al., 2020). As a result, the Ce(III)-doped g-C₃N₄ (Ce(III)-g-C₃N₄) possessed a high catalytic ozonation activity in oxalate degradation, which was ascribed to the synergistic effect of surface hydroxyl groups and Ce(III) active site.

Moreover, the LaCoO₃/g-C₃N₄ exhibited an outstanding activity in catalytic ozonation for the degradation of BZA due to the formation of electron transfer cycle Zhang et al., 2019b). The electron transfer cycle in LaCoO₃/g-C₃N₄, which was induced by the -C-O-Co bonding and nitrogen vacancy, could accelerate the decomposition of O₃ to generate more •OH, thus promoting the BZA degradation. As shown in Fig. 4a and b, the k_{obs} raised with the increase of the relative content of -C-O-Co bonding and nitrogen vacancy, indicating the positive role of -C-O-Co bonding and nitrogen vacancy in LaCoO₃/g-C₃N₄ in catalytic ozonation. The mechanism for LaCoO₃/g-C₃N₄ catalytic ozonation was displayed in Fig. 4c. First, the O₃ trapped the single electrons from nitrogen vacancies to generate •O₃⁻ (Eq. (3)). Meanwhile, the O₃ was decomposed by the -C-O-Co bonding to form •O₂⁻ and ¹O₂ (Eq. (9)). And the O₃ could react with OH⁻ to produce •O₂⁻ and HO₂• (Eq. (10)). Additionally, the O₂ captured the delocalized electrons from electron-rich centers to generate •O₂⁻ (Eq. (11)). Then, a series of radical chain reactions (Eqs. (4) and (12)) were induced by the •O₂⁻ and HO₂• to produce •OH (Eq. (5)). Thus the catalytic ozonation activity of LaCoO₃/g-C₃N₄ for BZA degradation was significantly improved.



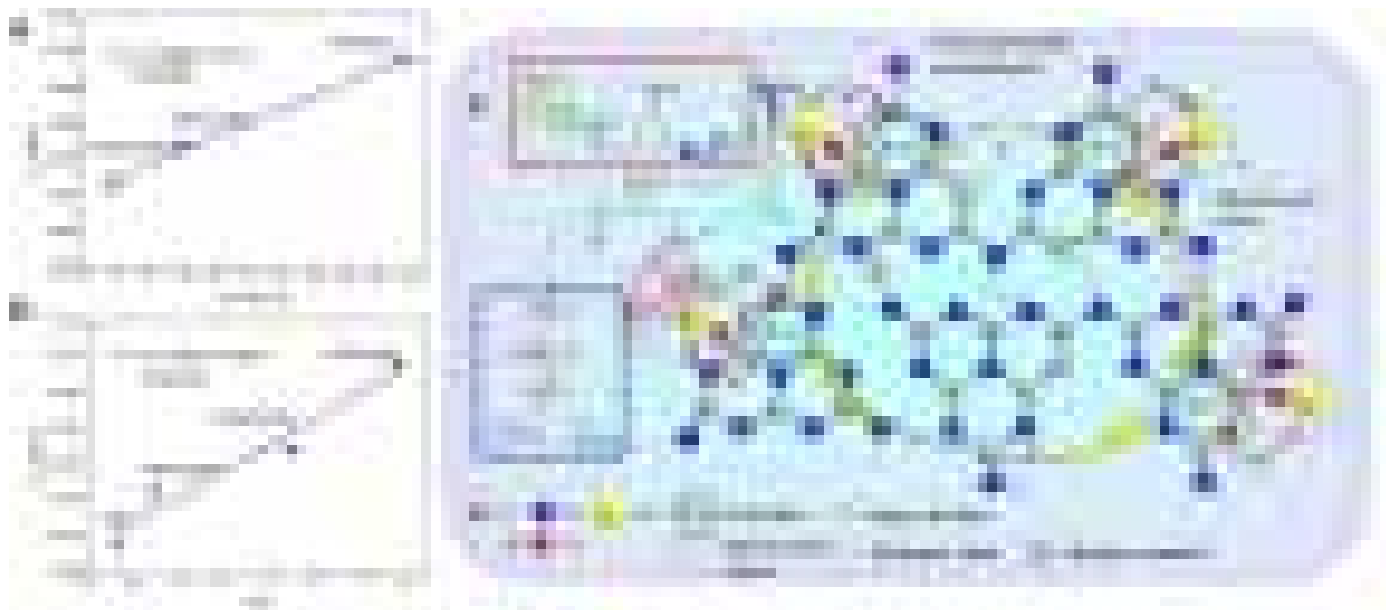


Fig. 4. (a) Effect of -C-O-Co relative content on the degradation efficiency of BZA and (b) effect of C/N on the degradation efficiency of BZA. (c) Reaction mechanism of catalytic ozonation with LaCoO₃/g-C₃N₄. Reproduced with permission from Ref. (Zhang et al., 2019b). Copyright 2019 Elsevier.

Furthermore, the g-C₃N₄-based catalysts were also utilized in O₃/H₂O₂ process to promote the formation of •OH under acidic conditions. In general, the production of •OH in O₃/H₂O₂ process is limited under acidic conditions as the HO₂⁻ that can induce free radical chain reactions to generate •OH is mainly formed under alkaline conditions (Li et al., 2015; Sein et al., 2008). To overcome this drawback, Guo et al. (2019) anchored single Mn atoms on g-C₃N₄ (Mn-CN) to accelerate the •OH formation for the degradation of oxalic acid (OA). As shown in Fig. 5a and b, the Mn-CN catalyst exhibited high activity for OA degradation in the O₃/H₂O₂ process, which was ascribed to the increased yield of •OH (Fig. 5c). The chronoamperometry curves (Fig. 5d) and EPR measurements (Fig. 5e) suggested that the HO₂• was formed in the interaction between Mn-CN and H₂O₂, and the O₃ could promote the formation of HO₂•. The energy change plot for different steps (Fig. 5f) further confirmed the reaction mechanism. During the reaction (Fig. 5g), the Mn-N₄ site in Mn-CN catalyst adsorbed H₂O₂ to form the HOO-Mn-N₄ species, which then reacted with O₃ to generate HO₂• and •O₃⁻. •O₃⁻ would combine with H⁺ in acidic solution to generate HO₃• and it rapidly transformed to •OH. Meanwhile, HO₂• converted to •O₂⁻, which could also react with O₃ to produce •O₃⁻. Therefore, the yield of •OH was increased and the degradation efficiency of OA was significantly enhanced.

The general catalytic mechanisms of g-C₃N₄-based catalysts during catalytic ozonation are presented in Fig. 1. In brief, the delocalized electrons and surface oxygen-containing functional groups on g-C₃N₄ can promote the transformation of O₃ to generate •OH and •O₂⁻. Additionally, the immobilized metal species on g-C₃N₄ also can activate O₃ to produce •OH, •O₂⁻ and ¹O₂. Consequently, these generated ROS will accelerate the degradation of organic pollutants.

4. Application of g-C₃N₄-based catalysts in persulfates activation

As an effective and promising technology for the degradation of organic pollutants in water, the AOPs based on persulfates including peroxymonosulfate (PMS, HS₅⁻) or peroxydisulfate (PDS, S₂O₈²⁻) have received increasing attention in recent years (Qin et al., 2020; Yu et al., 2020; Zhou et al., 2020b). Persulfates

are strong oxidants and the redox potential for PMS and PDS are 1.82 V and 2.01 V, respectively. Compared with H₂O₂ and O₃, the persulfates is more convenient for storage and transportation because they usually exist as solid power. However, their direct reaction with most organic pollutants is so slow, which need further activation for practical applications. In previous studies, numerous strategies such as UV, heat, alkali, ultrasound, transition metals and carbon-based catalysts have been utilized for persulfates activation, where reactive radicals (e.g., SO₄²⁻ and •OH) or nonradical species (¹O₂ and surface-bound complexes) are generated for effectively degrading organic pollutants (Liu et al., 2020b; Wang and Wang, 2018). Among these approaches, heterogeneous catalysis has attracted extensive interests due to its less energy consumption, high catalytic activity and outstanding reusability (Wu et al., 2019; Xiao et al., 2020). Therefore, many efforts have been devoted to exploring heterogeneous catalysts for persulfates activation.

Graphitic carbon nitride-based catalysts have been considered as effective catalysts for activating persulfates to degrade organic pollutants (Table 3). Normally, the catalytic activity of g-C₃N₄ in persulfates activation is originated from the nitrogen- or oxygen-containing functional groups, defective edges and sp² hybridized carbon network (Dong et al., 2016; Duan et al., 2015). However, the physicochemical properties of g-C₃N₄ prepared by different precursors and calcination procedures are usually somewhat different, which may affect their activity for the activation of persulfates. Guan et al. (2020) investigated the influences of different precursors (e.g., melamine, dicyandiamide and urea) and calcination atmosphere (e.g., air and N₂) on the catalytic activity of g-C₃N₄ in PMS activation. As shown in Fig. 6a and b, the obtained g-C₃N₄ catalysts exhibited different catalytic activities for PMS activation to degrade BPA, and the g-C₃N₄ prepared from melamine and calcined in N₂ possessed the best performance. The difference in their catalytic activities was because of the variation in the type and amount of active sites caused by the different preparation procedures. Generally, methanol (MeOH), p-BQ and L-histidine (L-his) were used as ROS scavengers for SO₄²⁻ and •OH, •O₂⁻, and ¹O₂, respectively (Gholami et al., 2020a; Xu et al., 2020). The quenching experiments (Fig. 6c) and EPR tests demonstrated that SO₄²⁻ and •OH rather than •O₂⁻ or ¹O₂ were the major ROS responsible

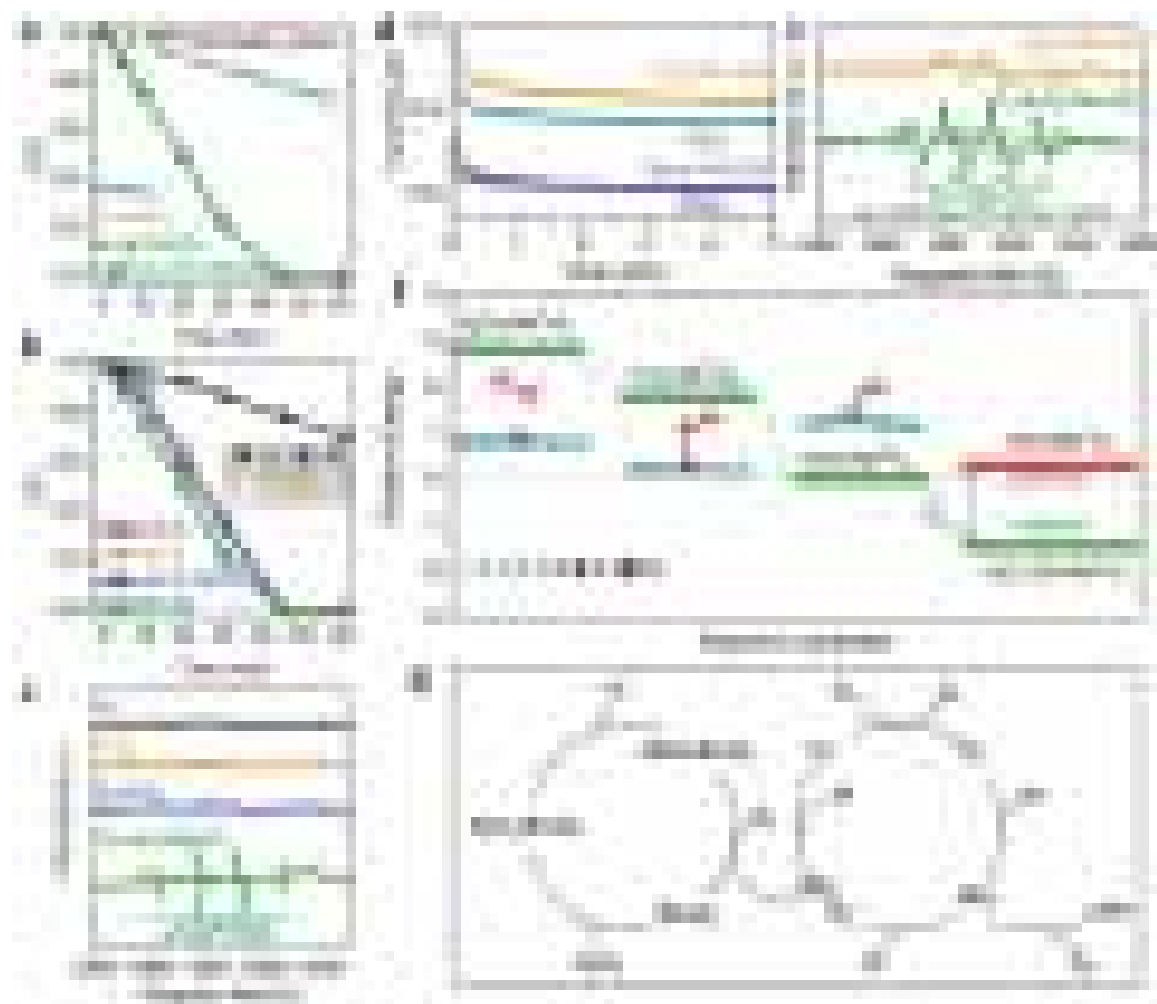


Fig. 5. (a) Degradation curves of OA in ozonation, the H₂O₂ process and the peroxone process with or without Mn-CN. (b) Degradation curves of OA in the peroxone process with g-C₃N₄, MnCl₂, a mixture composed of g-C₃N₄ and MnCl₂, or Mn-CN. (Inset: Corresponding solution color after reaction.) (c) EPR spectra of the DMPO-•OH adduct in ozonation, the H₂O₂ process, the peroxone process with Mn-CN. (d) Chronoamperometry curves in blank solution, blank solution with Mn-CN, H₂O₂ solution and H₂O₂ solution with Mn-CN. (e) EPR spectra of the DMPO- HO₂• adduct in the heterogeneous catalytic Fenton process and peroxone reaction with Mn-CN. (f) Free energy of H₂O₂ adsorption and HOO-Mn-N₄ detachment. (g) Reaction mechanism in the Mn-CN catalytic peroxone reaction. Reproduced with permission from Ref. (Guo et al., 2019). Copyright 2019 American Chemical Society.

Table 3
Catalytic activity of g-C₃N₄-based catalysts in persulfates activation.

Catalyst	Reaction conditions			pH	Catalytic efficiency			Key reactive species	Reference
	Pollutant [P]	[C]	[PS]		DE (min)	k _{obs} (min ⁻¹)	TOC (min)		
g-C ₃ N ₄ -M O-CN	BPA	10 μM	0.5 g L ⁻¹	PMS/1 mM	7	100% (40)	0.0982	36.4% (60)	SO ₄ • ⁻ , •OH
	BPA	0.05 mM	1.0 g L ⁻¹	PMS/10 mM	6.4	100% (45)	–	53% (60)	SO ₄ • ⁻ , •OH, SO ₄ • ⁻
g-C ₃ N ₄ /AC CN-CG	AO 7	50 mg L ⁻¹	0.2 g L ⁻¹	PMS/0.4 g L ⁻¹	3.82	96.4% (10)	–	8.2% (10)	•OH, SO ₄ • ⁻
	BPA	50 mg L ⁻¹	1.0 g L ⁻¹	PMS/0.27 mM	7	90% (30)	–	80% (30)	SO ₄ • ⁻ , •OH, SO ₄ • ⁻ , •OH, 'O ₂
Fe-g-C ₃ N ₄	Phenol	0.1 mM	1.0 g L ⁻¹	PMS/5 mM	2.6	100% (20)	~0.32	–	Fe ^{IV} =O
Fe(III)-g-C ₃ N ₄	4-CP	0.1 mM	0.1 g L ⁻¹	PMS/1 mM	3	100% (20)	~0.25	–	Fe ^V =O
Co-g-C ₃ N ₄	4-CP	50 mg L ⁻¹	1.0 g L ⁻¹	PMS/2.5 mM	–	100% (90)	0.062	32% (120)	SO ₄ • ⁻ , •OH
Mn-g-C ₃ N ₄	ACT	20 mg L ⁻¹	0.2 g L ⁻¹	PMS/0.8 g L ⁻¹	6.5	100% (15)	~0.31	–	'O ₂ , •O ₂ ⁻
FeO _y /S-g-C ₃ N ₄	SMX	10 mg L ⁻¹	0.2 g L ⁻¹	PMS/0.8 mM	3.54	100% (90)	0.06	43.9% (90)	SO ₄ • ⁻ , •OH, 'O ₂
Mn ₃ O ₄ /g-C ₃ N ₄	4-CP	50 mg L ⁻¹	0.3 g L ⁻¹	PMS/1 mM	–	100% (60)	0.0818	80% (60)	'O ₂ , SO ₄ • ⁻ , •OH
CoFeO ₂ /g-C ₃ N ₄ g-C ₃ N ₄ /MnFe ₂ O ₄	LVF	10 mg L ⁻¹	0.1 g L ⁻¹	PMS/0.5 mM	3	75% (5)	–	30% (5)	SO ₄ • ⁻
	TCS	9 mg L ⁻¹	0.2 g L ⁻¹	PMS/0.5 mM	11	97% (60)	0.0527	44.6% (60)	SO ₄ • ⁻ , •OH, SO ₄ • ⁻ , •O ₂ ⁻ , 'O ₂
FeCo ₂ S ₄ /g-C ₃ N ₄	SMX	19.7 μM	0.02 g L ⁻¹	PMS/0.15 mM	6.5	91.9% (15)	0.151	26.1% (15)	'O ₂

[P]: pollutant concentration; [C]: catalyst dosage; [PS]: persulfates concentration; DE: degradation efficiency; k_{obs}: apparent rate constant; TOC: total organic carbon; BPA: bisphenol A; AO 7: Acid Orange 7; 4-CP: 4-chlorophenol; ACT: acetaminophen; SMX: sulfamethoxazole; LVF: levofloxacin; TCS: triclosan.

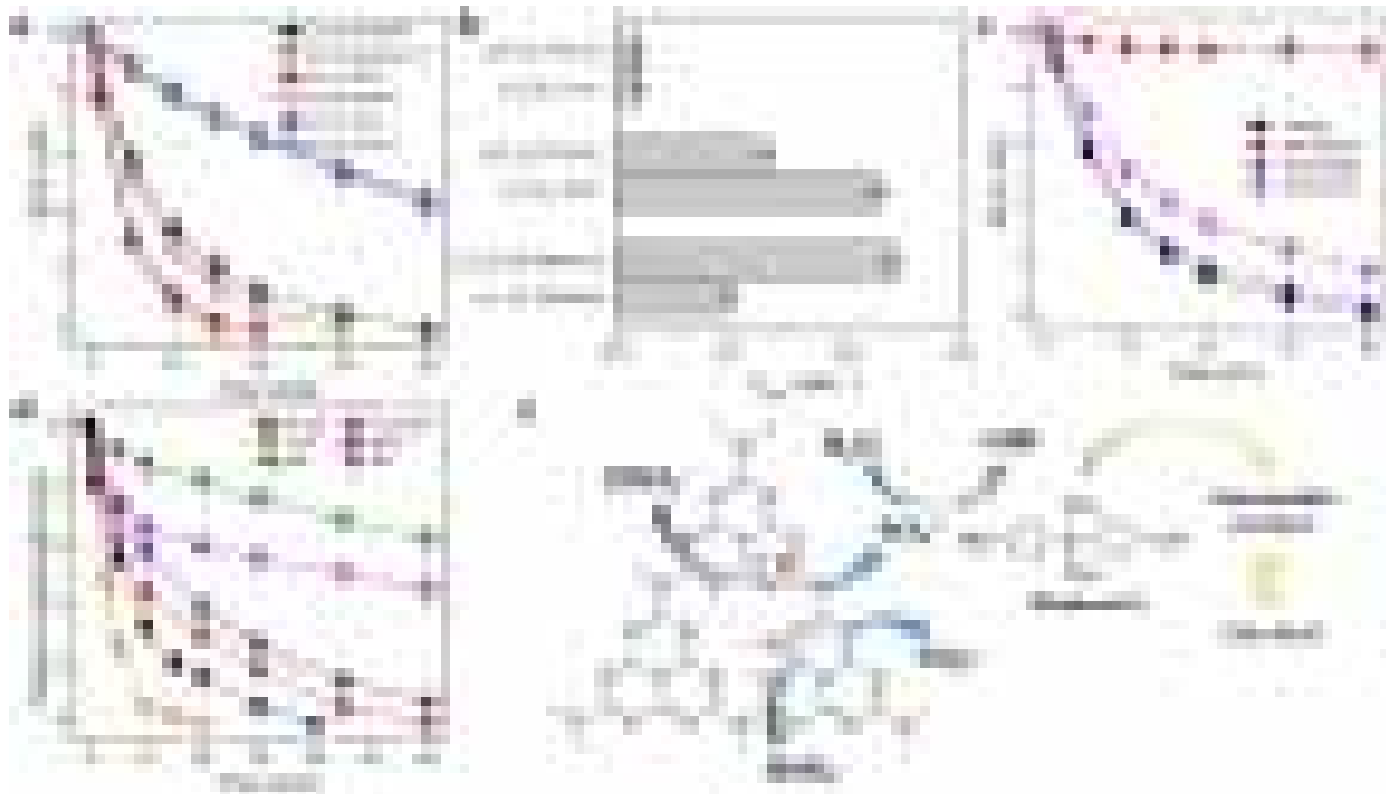


Fig. 6. (a) Time courses of BPA oxidation by PMS in the presence of the as-prepared g-C₃N₄ materials and (b) the k_{obs} for BPA oxidation. (c) Effects of MeOH, p-BQ or L-his on degradation of BPA by the g-C₃N₄-Melamine/PMS system. (d) Degradation of various organic compounds by the g-C₃N₄-Melamine/PMS system. (e) Mechanism of PMS activation by g-C₃N₄. Reproduced with permission from Ref. (Guan et al., 2020). Copyright 2020 Elsevier.

for the degradation of BPA. Meanwhile, the g-C₃N₄ also exhibited effective catalytic activity to degrade phenol, 2,4,6-tribromophenol (2,4,6-TBP), acetaminophen (ACT), sulfamethoxazole (SMX), ibuprofen (IPB) and benzoic acid (BA) via activating PMS (Fig. 6d), further excluding the contribution of surface-bound reactive complexes. Accordingly, the mechanism of PMS activation by g-C₃N₄ was proposed in Fig. 6e. First, PMS was decomposed by the active sites on the surface of g-C₃N₄ via an electron transfer pathway to form SO₄^{•-} (Eq. (13)) and SO₅^{•-} (Eq. (14)). Then the SO₄^{•-} could react with H₂O to generate •OH (Eq. (15)), while the SO₅^{•-} could self-react to generate SO₄^{•-} (Eq. (16)), resulting in the BPA degradation.



However, the catalytic performance of pure g-C₃N₄ in persulfates activation is greatly suppressed by its poor electron transfer capability (Lin et al., 2018b). To improve the electron mobility of g-C₃N₄ for efficiently activating persulfates, Gao et al. (2018b) prepared O-doped g-C₃N₄ (O-CN) with modulated electronic structure. As displayed in Fig. 7a and b, compared with pure g-C₃N₄, the electronic structure of O-CN was altered due to the substitution of N atoms by O atoms. Because the electronegativity of O atom is higher than that of C atom and N atom, the electrons of C atoms would flow to the O atom, leading to formation of high and low electron density regions around the O atom and C atom, respectively. Consequently,

the electron transfer on O-CN would be accelerated, which was confirmed by the electrochemical impedance spectroscopy (EIS) spectra (Fig. 7c). Benefiting from the modulated electronic structure, the O-CN exhibited excellent catalytic activity in PMS activation for the degradation of BPA, CIP and 2-chlorophenol (2-CP). The EPR tests and quenching experiments (Fig. 7d) indicated that the O-CN could activate PMS to generate SO₄^{•-}, •OH and ¹O₂, in which ¹O₂ was the major ROS responsible for BPA degradation. The N₂-saturated experiment and linear sweep voltammetry (LSV) analysis (Fig. 7e) further demonstrated that ¹O₂ was originated from the PMS oxidation rather than from the conversion of •O₂^{•-}. Therefore, the mechanism of PMS activation by O-CN could be proposed, as depicted in Fig. 7f. The one was the PMS oxidation by electron-poor C atoms to form SO₅^{•-}, followed by the reaction between SO₅^{•-} and H₂O to generate ¹O₂. The other was the PMS reduction by the electrons around the electron-rich O atoms to generate SO₄^{•-} and •OH.

As many metal species can activate persulfates to degrade organic pollutants, it is reasonable to expect that incorporation of metal species could effectively enhance the catalytic performance of g-C₃N₄ towards persulfates activation (Li et al., 2017; Oh et al., 2017; Zhang et al., 2019a). Meanwhile, the unique structure of g-C₃N₄ with two-dimensional layered nanosheets and six nitrogen lone-pair electrons is conductive to the immobilization and dispersion of metal species. Therefore, many efforts have been devoted to incorporating metal species into g-C₃N₄ for enhancing persulfates activation (Nguyen et al., 2019; Qin et al., 2019; Yang et al., 2019a). For example, Xie et al. (2019) synthesized Co-doped g-C₃N₄ (Co-g-C₃N₄) for PMS activation to degrade monochlorophenols (MCPs) isomers, including 2-CP, 3-chlorophenol (3-CP) and 4-chlorophenol (4-CP). The Co-g-C₃N₄ exhibited superior catalytic activity in PMS activation compared with g-C₃N₄ due to the doping of Co. The Co

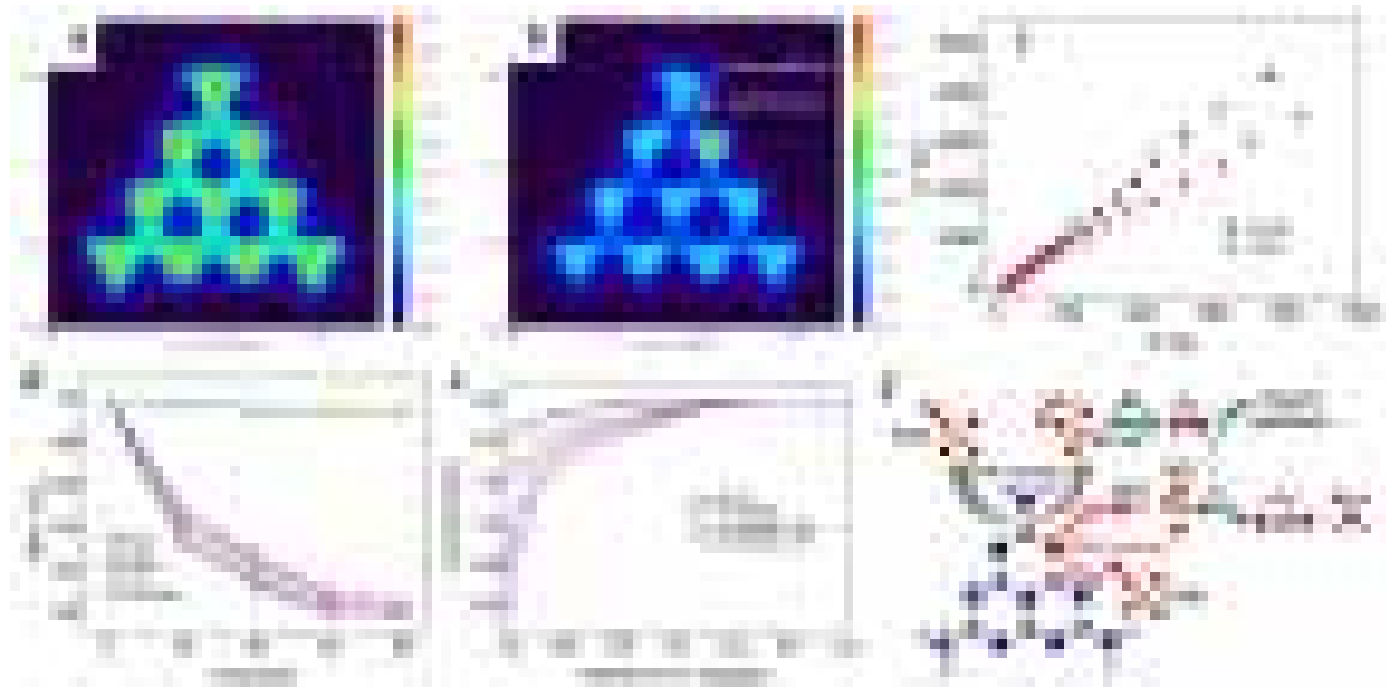
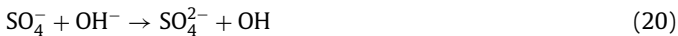
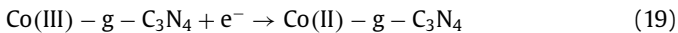
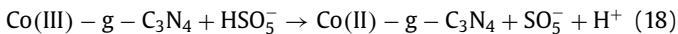
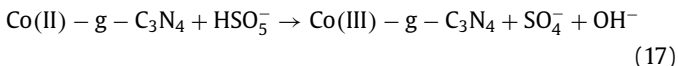


Fig. 7. Two-dimensional valence-electron density color-filled maps of (a) g-C₃N₄ and (b) O-CN. (c) EIS spectra of g-C₃N₄ and O-CN. (d) Effect of scavengers on catalytic degradation of BPA in the O-CN/PMS system. (e) LSV curves of O-CN with and without PMS and BPA or DP. (f) Mechanism of PMS activation by O-CN. Reproduced with permission from Ref. (Gao et al., 2018b). Copyright 2018 American Chemical Society.

doping could promote the generation of SO₄²⁻ (Eqs. (17)–(20)), resulting in the improved degradation of MCPs. Meanwhile, the adsorption experiments and quantum chemical calculations demonstrated that the adsorption behavior based on the intermolecular interactions between Co-g-C₃N₄ and MCPs was benefit to the process of MCPs degradation. Fan et al. (2019) prepared Mn-doped g-C₃N₄ (Mn-g-C₃N₄) to activate PMS for the degradation of ACT. The catalytic performance of g-C₃N₄ was significantly improved by the doping of Mn. Further researches demonstrated that ¹O₂ rather than SO₄²⁻ or •OH was the active species responsible for the degradation of ACT. In addition to transition metal species, noble metal species were also introduced into g-C₃N₄ (Feng et al., 2018a). Wang et al. (2017) found that Pd nanoparticles could greatly enhance the performance of g-C₃N₄ in PMS activation to degrade BPA because it could promote the formation of surface-bound radical intermediates.



Interestingly, it has been found that high-valent iron-oxo species (e.g., Fe^{IV}=O and Fe^V=O) instead of ROS (e.g., SO₄²⁻, •OH and ¹O₂) were responsible for the degradation of organic pollutants in persulfates activation by Fe-g-C₃N₄ (Li et al., 2019a). For example, Feng et al. (2018b) synthesized Fe(II)-g-C₃N₄ to activate PMS for the degradation of phenol. Compared with g-C₃N₄, the Fe(II)-g-C₃N₄ possessed superior catalytic activity in PMS activation to degrade phenol, which was attributed to the formation of Fe^{IV}=O. The Fe^{IV}=O could rapidly degrade the phenol through electron

transfer. Li et al. (2018) employed Fe(III)-doped g-C₃N₄ (Fe(III)-g-C₃N₄) to activate PMS for the degradation of 4-CP. As shown in Fig. 8a, the degradation efficiency of 4-CP increased with the increase of Fe(III) content in Fe(III)-g-C₃N₄. When oxalate and citrate were added, the degradation efficiency of 4-CP was decreased (Fig. 8b and c). These results suggested that the embedded Fe(III) in g-C₃N₄ framework acted as the active sites for 4-CP degradation. Moreover, the EPR test and quenching experiments demonstrated that traditional ROS in persulfates activation (e.g., SO₄²⁻, •OH and ¹O₂) played an insignificant role in degrading 4-CP. However, the degradation efficiency of 4-CP was suppressed by adding the dimethyl sulfoxide (DMSO) (Fig. 8d), which is a probe compound for high-valent iron-oxo species. The DMSO can be oxidized by the high-valent iron-oxo species to generate the dimethyl sulfone (DMSO₂). Accordingly, it could be concluded that the Fe^V=O was formed on Fe(III)-g-C₃N₄ in PMS activation, resulting in the 4-CP degradation via nonradical pathway, as described in Fig. 8e.

In comparison with monometallic species, bimetallic species have a better catalytic activity for persulfates activation because of the strengthened synergistic effect of metallic elements and the presence of abundant redox reactions Chen et al., 2017; Lei et al., 2020b; Lin et al., 2018a). Thus, a series of bimetallic species have been incorporated into g-C₃N₄ to activate persulfates. For example, Pi et al. (2020) synthesized CoFeO₂/g-C₃N₄ to activate PMS for the degradation of levofloxacin (LVF). The CoFeO₂/g-C₃N₄ displayed a higher catalytic performance than CoFeO₂ in activating PMS to degrade LVF due to the accelerated redox cycles of metal species. During the reaction, Co(II) and Fe(III) activated HS₂O₅⁻ to form SO₄²⁻ (Eqs. (21) and (22)), while Fe(II) and Co(III) activated HS₂O₅⁻ to form SO₅²⁻ (Eqs. (23) and (24)), resulting in the LVF degradation. Li et al. (2020d) fabricated FeCo₂S₄/g-C₃N₄ to degrade SMX through the activation of PMS. Owing to the synergistic effect between FeCo₂S₄ and g-C₃N₄, the catalytic activity of FeCo₂S₄/g-C₃N₄ was superior to FeCo₂S₄, g-C₃N₄ and Co₃S₄/g-C₃N₄. The degradation efficiency of SMX was determined to be 60.1%, 17.8%, 73.9% and 91.9% for FeCo₂S₄, g-C₃N₄, Co₃S₄/g-C₃N₄ and FeCo₂S₄/g-

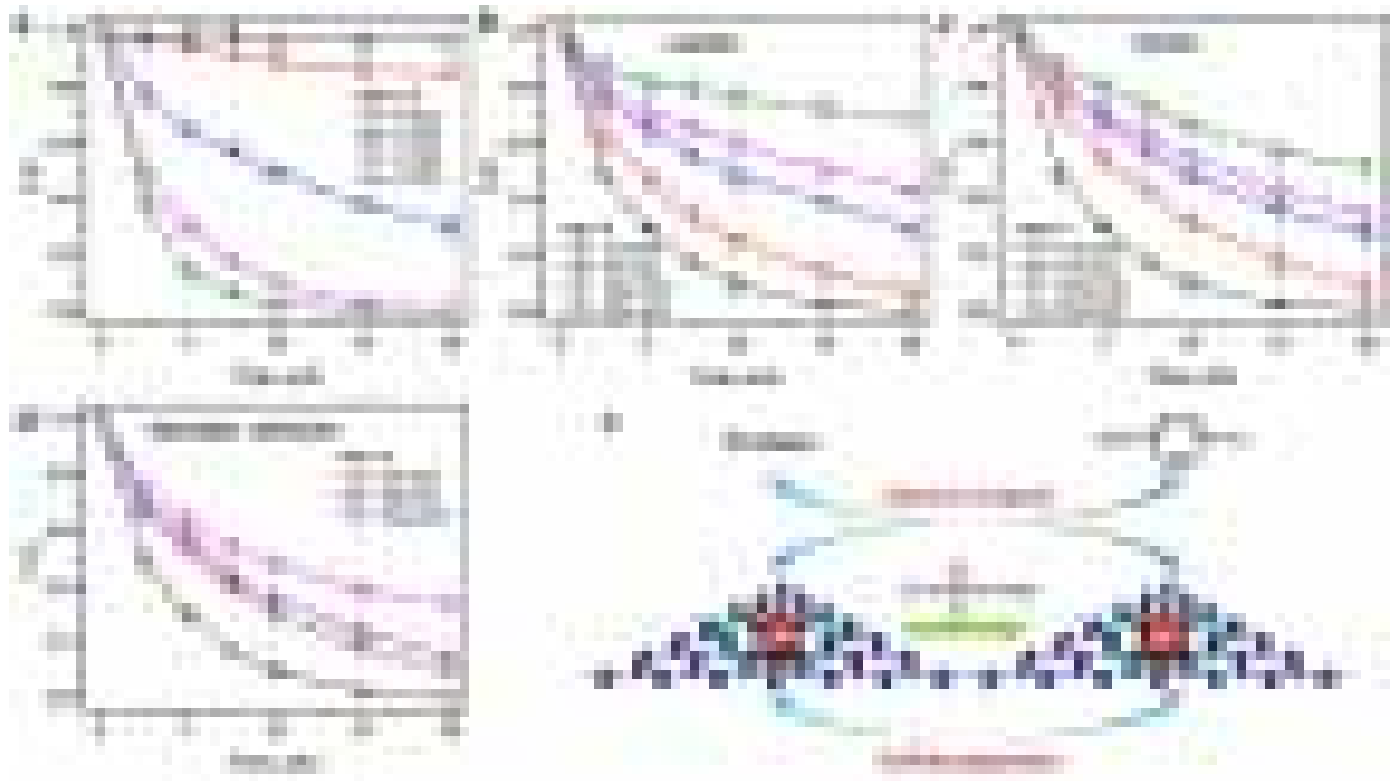
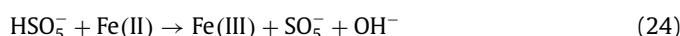
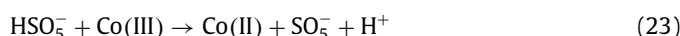
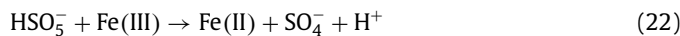
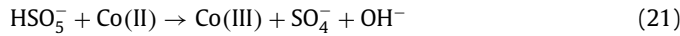


Fig. 8. (a) Degradation of 4-CP in different PMS/Fe(III)-g-C₃N₄ systems. Effects of (b) oxalate and (c) citrate on 4-CP degradation in the PMS/Fe(III)-g-C₃N₄ system. (d) Effect of DMSO on 4-CP degradation in the PMS/Fe(III)-g-C₃N₄ system. (e) Mechanism of PMS activation by Fe(III)-g-C₃N₄. Reproduced with permission from Ref. (Li et al., 2018). Copyright 2018 American Chemical Society.

C₃N₄, respectively. For FeCo₂S₄/g-C₃N₄, ¹O₂ was identified to be the dominant active species responsible for SMX degradation.



Additionally, metal-free materials with high electrical conductivity were employed to accelerate the electron transfer on g-C₃N₄ for enhancing the activation of persulfates (Chen et al., 2018; Guo et al., 2018; Ye et al., 2019b). For example, Wei et al. (2016) combined g-C₃N₄ with activated carbon (AC) to activate PMS for the degradation of organic pollutants. Compared with g-C₃N₄ and AC, the g-C₃N₄/AC composite exhibited superior catalytic activity in PMS activation to degrade Acid Orange 7 (AO 7), which was ascribed to the synergistic effect between g-C₃N₄ and AC. Firstly, the specific surface area of g-C₃N₄/AC was larger than that of g-C₃N₄, which could provide more active sites and increase the adsorption ability for AO 7. Secondly, the effective interfacial contact between g-C₃N₄ and AC could greatly facilitate the electron transfer on g-C₃N₄. Therefore, both the radical generation (SO₄^{•-} and •OH) and the nonradical effect in PMS activation were significantly enhanced, resulting in the efficient degradation of organic pollutants. Yao et al. (2019) introduced covalent organic framework (COF) into g-C₃N₄ to promote PMS activation for the degradation of Orange II. The electron transfer between g-C₃N₄@COF and PMS was boosted, which was attributed to the good balance between nitrogen content and graphitization degree. As a

result, the g-C₃N₄@COF showed excellent catalytic activity in PMS activation to degrade Orange II because of the strengthened non-radical pathway induced by boosted electron transfer.

Recently, the combination of photocatalysis and persulfates activation has drawn increasing attention because the synergistic effect between them could significantly improve the catalytic performance (Gao et al., 2017; Wang et al., 2020d; Yang et al., 2019b). Normally, the persulfates can be activated by the photogenerated electrons on g-C₃N₄-based catalysts to generate SO₄^{•-} and •OH, resulting in the boosted persulfates activation and enhanced organic pollutants degradation. For example, Gao et al. (2018a) utilized a Co₃O₄ QDs/g-C₃N₄ heterostructure to degrade TC under visible light in the presence of PMS. Compared to the case without visible light or PMS, the degradation efficiency was greatly enhanced, which was ascribed to the cooperative effect between photocatalysis and persulfates activation. In the study of Li et al. (2019d), the CuFe₂O₄/g-C₃N₄ composite exhibited improved catalytic performance on PDS activation under visible light for the degradation of propranolol due to the self-redox cycles of iron and copper in CuFe₂O₄ and the accelerated formation of SO₄^{•-}. Moreover, our group recently developed a novel carbonyl and carboxyl groups co-modified g-C₃N₄ and employed it for the PMS activation under visible light to degrade chlortetracycline hydrochloride (Guo et al., 2020b). In this system, the photogenerated electrons were gathered around the electron-withdrawing carbonyl and carboxyl groups of g-C₃N₄. The PMS could be quickly activated by these electrons to generate SO₄^{•-} and •OH, leading to the efficient degradation of chlortetracycline hydrochloride.

The general catalytic mechanisms of g-C₃N₄-based catalysts during persulfates activation are displayed in Fig. 1. In short, the nitrogen- or oxygen-containing functional groups, defective edges, sp² hybridized carbon network and photogenerated electrons of g-C₃N₄ can facilitate the decomposition of persulfates to produce

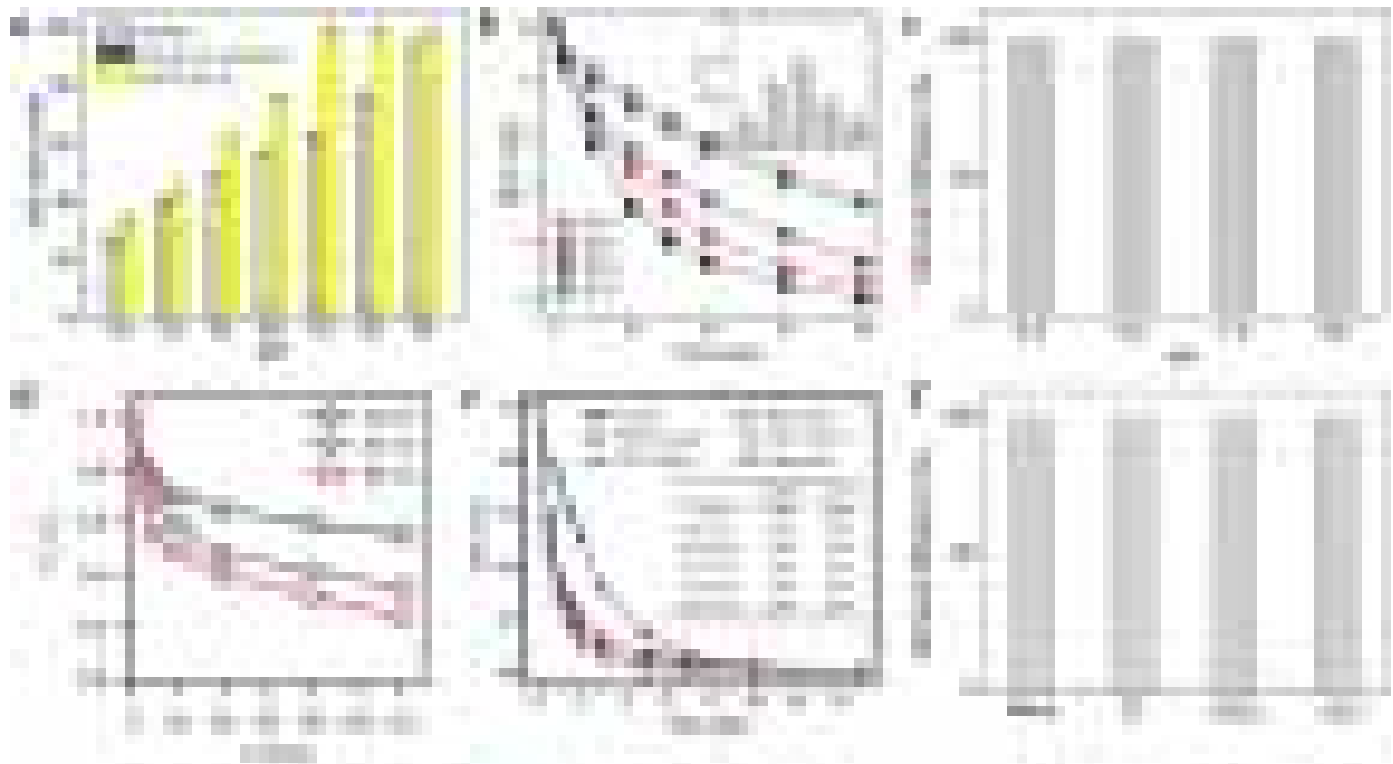


Fig. 9. (a) Effect of solution pH on the degradation of ATZ in the ZVZ-g-C₃N₄/O₃ system. Reproduced with permission from Ref. (Yuan et al., 2018b). Copyright 2018 Elsevier. (b) Effect of solution pH on the degradation of BPA in the g-C₃N₄-Melamine/PMS system. Reproduced with permission from Ref. (Guan et al., 2020). Copyright 2020 Elsevier. Effect of (c) solution pH and (f) common inorganic anions on the degradation of BPA in the O-CN/PMS system. Reproduced with permission from Ref. (Gao et al., 2018b). Copyright 2018 American Chemical Society. (d) Effect of temperature on the degradation of RhB in the S-g-C₃N₄/PDS system. Reproduced with permission from Ref. (Lin et al., 2018b). Copyright 2018 Elsevier. (e) Effect of NOM on the degradation of ATZ in the O@g-C₃N₄/O₃ system. Reproduced with permission from Ref. (Yuan et al., 2019). Copyright 2019 Elsevier.

SO₄•⁻ and •OH. Moreover, the loaded metal species on g-C₃N₄ also can activate persulfates to generate SO₄•⁻, •OH, •O₂⁻ and ¹O₂. Especially, the Fe-N complex on Fe-g-C₃N₄ can bind to PMS, resulting in the formation of high-valent iron-oxo species. As a result, these reactive species will promote the degradation of organic pollutants.

5. The effect of water chemistry on catalytic performance

5.1. Effect of pH

Due to the variable pH values of actual wastewater, it is very important to clarify the effect of pH on the performance of g-C₃N₄-based catalysts in AOPs. Normally, the solution pH affects the surface properties of g-C₃N₄-based catalysts, the structural forms of target contaminants and the decomposition of oxidants (H₂O₂, O₃ and persulfates), thereby influencing the catalytic performance. The pH at point of zero charge (pH_{pzc}) can help determine the effect of pH on the surface charge of the catalyst. When the solution pH is less than pH_{pzc}, the surface of the catalyst is positively charged, and when the solution pH is greater than pH_{pzc}, the surface of the catalyst is negatively charged. For example, the pH_{pzc} of zero-valent zinc immobilized g-C₃N₄ (ZVZ-g-C₃N₄) was determined to be 5.96 (Yuan et al., 2018b). At the initial pH above pH_{pzc}, the surface of the catalyst was negatively charged as [ZVZ-g-C₃N₄]-O⁻ group. Therefore, the ZVZ-g-C₃N₄ showed superior catalytic ozonation performance on ATZ degradation in the pH range of 7.0–9.0 since O₃ is more likely to react with negatively charged surface (Fig. 9a). In the study of Li et al. (2020d), the pH_{pzc} of FeCo₂S₄/g-C₃N₄ was determined to be 5.9. Accordingly, at the initial pH of 3.5 or 5.0 and 6.5, 8.0 or 9.5, the surface charge of FeCo₂S₄/g-C₃N₄

was positive and negative, respectively. Because the SMX existed as anionic species in the pH range of 3.5–9.5, the interaction between FeCo₂S₄/g-C₃N₄ and SMX was enhanced at the initial pH of 3.5 and 5.0, promoting the degradation of SMX in the presence of PMS.

In addition, the decomposition of oxidants are also influenced by the solution pH. In alkali media, the oxidability of H₂O₂ is weakened because of its decomposition to O₂ and H₂O (Cheng et al., 2018a). The activity of O₃ alone for organic pollutants degradation under acidic conditions is unsatisfactory. However, at high pH, the abundant OH⁻ can react with O₃ to accelerate the formation of •OH, thus promoting the degradation of organic pollutants (Nawrocki and Kasprowski, 2010; Wang and Chen, 2020). Moreover, the PMS will decomposed to SO₄²⁻, O₂ and H₂O at high pH, inhibiting the generation of ROS (Ball and Edwards, 1956). As shown in Fig. 9b, in the g-C₃N₄/PMS system, the k_{obs} of BPA degradation increased with pH increasing from 5.0 to 7.0, and then decreased as pH further increased to 9.0 (Guan et al., 2020). This phenomenon could be ascribed to the following reasons. At lower pH values, the electron transfer from g-C₃N₄ surface to PMS was inhibited. Moreover, the alkaline conditions weakened the interaction between g-C₃N₄ surface and HSO₅⁻ and accelerated the self-decomposition of PMS.

Nonetheless, most of the g-C₃N₄-based catalysts were applicable in a wide pH range for the degradation of organic pollutants. For example, Gao et al. (2018b) reported that PMS could be activated by O-CN in a wide pH range of 3.0–9.0 to efficiently degrade BPA (Fig. 9c). The ZnO/g-C₃N₄ exhibited excellent activity in a wide pH range of 3.5–9.5 for ATZ degradation in catalytic ozonation (Yuan et al., 2018a). The degradation efficiency of ATZ at each pH value was all over 95.5% within 3 min, indicating the slight ef-

fect of solution pH on the ATZ degradation. Normally, the classical Fenton reaction only works better under acidic conditions because it easily forms iron precipitates under neutral and alkaline conditions. Compared to recent novel heterogeneous Fenton-like catalysts such as Fe-Pd@C (He et al., 2019a) and nFe₂O₃/MIL-53(Cu) (Ren et al., 2020), which only worked in a narrow pH range of 3.0–6.0, the g-C₃N₄-based catalysts usually performed well in a wider pH range. For example, in the study of Lyu et al. (2018), the CN-Cu(II)-CuAlO₂ catalyst exhibited effective activity for BPA degradation in a wide pH range of 5.0–9.0, and possessed the highest activity under the neutral conditions. No significant variation in the removal efficiency of BPA could be observed in the pH range of 5.0–7.0 with the change of initial pH. And although the removal efficiency of BPA slightly decreased with the increase of initial pH in the pH range of 7.0–9.0, it could still achieve 70% at pH 9.0 after 120 min reaction, which was attributed to its dual reaction centers. Moreover, the Cu(I)-g-C₃N₄ also displayed satisfactory activity for the degradation of RhB in a wide pH range of 5.0–11.0 (Ma et al., 2019b). Unlike traditional Fenton-like reactions, the removal efficiency of RhB increased with the increase of solution pH in the pH range of 3.0–6.0, while remained almost unchanged as the pH further increased to 11.0. The efficient activity of Cu(I)-g-C₃N₄ for RhB degradation at higher pH values was ascribed to the ¹O₂, which was more easily generated under the alkaline conditions than the acidic conditions.

5.2. Effect of water temperature

At ambient temperature, the g-C₃N₄-based catalysts can perform well in Fenton-based processes, catalytic ozonation and persulfates activation. Slight temperature changes will not obviously affect the performance of g-C₃N₄-based catalysts for degrading organic pollutants through these AOPs. For example, the degradation efficiencies of BPA in the CN-Cu(II)-CuAlO₂/H₂O₂ system at 25 °C, 30 °C and 35 °C were 90%, 93% and 96%, respectively (Lyu et al., 2018). However, if the water temperature fluctuates greatly, the degradation rate of organic pollutants will also change significantly, especially in persulfates activation because heat is an effective method to activate persulfates. Lin et al. (2018b) utilized S-doped g-C₃N₄ (S-g-C₃N₄) to activate PDS for the degradation of RhB. As shown in Fig. 9d, the *k*_{obs} of RhB degradation was increased from 0.005 min⁻¹ to 0.014 min⁻¹ as the temperature was raised from 20 °C to 60 °C. Moreover, in the FeCo₂S₄/g-C₃N₄/PMS system, with the rise of temperature from 10 °C to 40 °C, the degradation efficiency of SMX was remarkably increased from 61.2% to 99.9%, and the *k*_{obs} of SMX degradation was also increased from 0.059 min⁻¹ to 0.294 min⁻¹ (Li et al., 2020d).

5.3. Effect of natural organic matter

Natural organic matter (NOM) is a complex mixture of organic substances, which is extensively distributed in ground water, surface water and wastewater. In AOPs, the NOM usually competes with target organic pollutants for ROS, leading to the reduction in degradation efficiency. As a major constituent of NOM, humic acid (HA) can react with O₃, which may depress the performance of catalytic ozonation. In the ZnO/g-C₃N₄/O₃ system, the *k*_{obs} of ATZ degradation decreased from 1.84 to 0.57 min⁻¹ when the HA concentration increased from 1.0 to 10.0 mg L⁻¹, which was ascribed to the competition between HA and ATZ for both O₃ and ROS (Yuan et al., 2018a). However, in the O@g-C₃N₄/O₃ system (Fig. 9e), the production of •OH was increased owing to the reaction between electron-rich moieties of HA and O₃, resulting in the accelerated ATZ degradation (Yuan et al., 2019). In addition, the NOM can also inhibit the g-C₃N₄-based catalysts to active persulfates because its abundant hydroxyl and carboxyl groups retard the

reaction between persulfates and g-C₃N₄-based catalysts to generate reactive species. For example, in the Fe(III)-g-C₃N₄/PMS system, the degradation efficiency of 4-CP declined from 93% to 72% with NOM concentration increasing from 1.0 to 20.0 mg L⁻¹ (Li et al., 2018). This was mainly because of the delayed reaction between PMS and Fe(III)-g-C₃N₄ caused by NOM as well as the competitive reaction between NOM and 4-CP.

5.4. Effect of inorganic anions

Inorganic anions are also ubiquitous in ground water, surface water and wastewater, which can serve as radical scavengers, resulting in an inhibitory effect on the radical-based degradation of organic pollutants. For example, in the ZVZ-g-C₃N₄/O₃ system, the HCO₃⁻ obviously suppressed ATZ degradation since the •OH was scavenged by HCO₃⁻ (Yuan et al., 2018b). In the g-C₃N₄/MnFe₂O₄/PMS system, the triclosan (TCS) degradation was inhibited by the HCO₃⁻ and low concentration of Cl⁻, which was attributed to the formation of less reactive radical species, such as •HCO₃, •CO₃⁻ and •Cl. While the high concentration of Cl⁻ could promote the degradation of TCS because of the generation of strong oxidizing species, such as Cl₂ and HOCl (Wang et al., 2019c). Besides, the effect of inorganic anions on organic contaminants degradation in the nonradical dominated process is usually insignificant. In the FeCo₂S₄/g-C₃N₄/PMS system, the ¹O₂ dominated nonradical pathway was determined to be the major process for SMX degradation. Thus, the Cl⁻, HCO₃⁻ and H₂PO₄⁻ showed unremarkable impact on the degradation of SMX (Li et al., 2020d). Similarly, as exhibited in Fig. 9f, in the O-CN/PMS system with ¹O₂ as the major ROS, the effect of Cl⁻, HCO₃⁻ and CO₃²⁻ on the degradation of BPA was negligible (Gao et al., 2018b). However, in PMS activation, some inorganic anions such as H₂PO₄⁻ (Li et al., 2019a) and F⁻ (Li et al., 2018) would hinder the formation of high-valent iron-oxo species due to the complexation between inorganic anions and iron species, leading to a slight decline in degradation efficiency.

5.5. Effect of dissolved oxygen

Dissolved oxygen (DO) is one of the essential parameters of water chemistry. It has been found that DO could get involved in the free radical chain reactions, thereby influencing the degradation of organic pollutants (Fang et al., 2013; Lu et al., 2019). Generally, as an electron acceptor, DO can react with one electron of catalysts to form •O₂⁻, which can be further reduced to H₂O₂ when two protons are present (Nosaka and Nosaka, 2017). Besides, the process of persulfates activation can also be affected by DO (Zhang et al., 2018; Zhu et al., 2018). However, there are limited reports on the effect of DO on the performance of g-C₃N₄-based catalysts in these AOPs. Meanwhile, these reports demonstrated that the effect of DO in the Fenton-based processes and persulfates activation over g-C₃N₄-based catalysts was insignificant. For example, in the CDs/Fe(II)-g-C₃N₄/H₂O₂ system (Fang et al., 2019), there was no obvious change in the degradation efficiency of MB in the absence of O₂. Moreover, in the O-CN/PMS system (Gao et al., 2018b), the BPA degradation was not inhibited after N₂ saturation, implying that the ¹O₂ was not derived from the DO in reaction solution.

6. Reusability, stability and toxicity

From the view of practical applications, the reusability and stability of g-C₃N₄-based catalysts in these AOPs are vital for the treatment of wastewater. Normally, the g-C₃N₄-based catalysts could still keep good catalytic performance after multiple successive cycles. For example, in Fenton-like oxidation, the catalytic activity of Cu-Al₂O₃-g-C₃N₄ for RhB degradation decreased

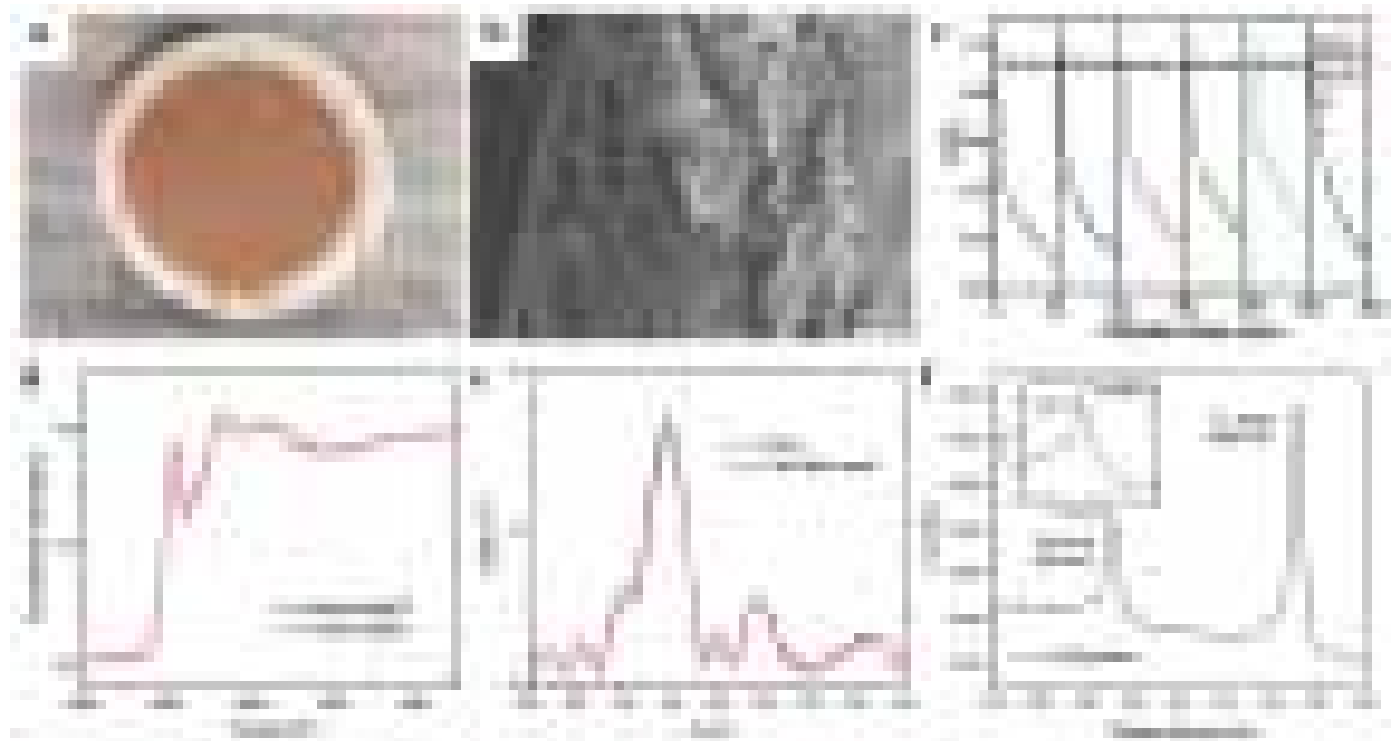


Fig. 10. (a) The digital image and (b) cross-sectional SEM of $\text{Mn}_3\text{O}_4/\text{g-C}_3\text{N}_4$ @PTFE membrane. (c) The reusability of $\text{Mn}_3\text{O}_4/\text{g-C}_3\text{N}_4$ @PTFE membrane for 4-CP degradation in the presence of PMS. Reproduced with permission from Ref. (Chen et al., 2020a). Copyright 2020 Elsevier. The comparison of (d) XANES and (e) EXAFS spectra at the Cu K-edge between the fresh Cu(I)- $\text{g-C}_3\text{N}_4$ and the catalyst after the degradation reaction. (f) XPS spectra of Cu 2p and Cu LMM Auger electron spectra (insert graph) of the used Cu(I)- $\text{g-C}_3\text{N}_4$. Reproduced with permission from Ref. (Ma et al., 2019b). Copyright 2019 Elsevier.

insignificantly after 7 successive cycles, reaching a removal efficiency of 91% in 60 min (Xu et al., 2018). In catalytic ozonation, the decline of the catalytic performance of $\text{CuO}/\text{g-C}_3\text{N}_4$ for OA degradation was not obvious after 5 successive cycles (Liu et al., 2020a). In PMS activation, 90% removal of TCS was obtained over $\text{g-C}_3\text{N}_4/\text{MnFe}_2\text{O}_4$ after 5 successive cycles (Wang et al., 2019c). In these cycles at lab-scale, centrifugation recovery and magnetic recovery were usually utilized to recover catalyst powder from the reaction suspension. However, in practical applications, they may be complicated and expensive because of the need to install a large capacity centrifuge or a large electromagnetic system. Recently, catalytic membranes have drawn considerable interest in practical applications due to the simple operation with no need to recover catalyst. Chen et al. (2020a) fabricated a $\text{Mn}_3\text{O}_4/\text{g-C}_3\text{N}_4$ @Polytetrafluoroethylene (PTFE) membrane via a facile vacuum filtration method and used it to activate PMS for 4-CP degradation (Fig. 10a and b). As shown in Fig. 10c, the catalytic performance of $\text{Mn}_3\text{O}_4/\text{g-C}_3\text{N}_4$ @PTFE membrane still maintained at high level after 5 successive cycles and was able to remove 80% of 4-CP in 60 min.

The stability of $\text{g-C}_3\text{N}_4$ -based catalysts in these AOPs was also confirmed by a series of characterizations, such as X-ray diffraction (XRD), X-ray photoelectron spectroscopy (XPS), Fourier transform infrared spectroscopy (FTIR), scanning electron microscopy (SEM) and transmission electron microscopy (TEM). In the study of Ma et al. (2019b), the XANES spectra and EXAFS spectra showed that the chemical state and coordination structure of the Cu in Cu(I)- $\text{g-C}_3\text{N}_4$ had no apparent changes before and after reaction (Fig. 10d and e). The XPS spectra also indicated that the Cu(I) was stably existed in $\text{g-C}_3\text{N}_4$ via N coordination after reaction (Fig. 10f). Moreover, it has been reported that $\text{g-C}_3\text{N}_4$ was chemically stable toward $\bullet\text{O}_2^-$ and O_3 (Xiao et al., 2017). And although $\bullet\text{OH}$ can di-

rectly tear the heptazine unit from $\text{g-C}_3\text{N}_4$ to generate secondary pollutants, the presence of organic pollutants will hinder the fragmentation of $\text{g-C}_3\text{N}_4$. In the study of Song et al. (2019b), the SEM, TEM and atomic force microscopy (AFM) images as well as the XRD and Raman spectra displayed that the morphology, crystal structure and framework of $\text{g-C}_3\text{N}_4$ were only slightly changed after catalytic ozonation, suggesting the high stability of $\text{g-C}_3\text{N}_4$. And EPR spectra exhibited that the amount of delocalized electrons in $\text{g-C}_3\text{N}_4$ decreased not obviously after catalytic ozonation, further verifying the relative chemical stability of $\text{g-C}_3\text{N}_4$. Overall, these results demonstrated the good reusability and stability of $\text{g-C}_3\text{N}_4$ -based catalysts in these AOPs for the degradation of organic contaminants.

Additionally, the toxicity of $\text{g-C}_3\text{N}_4$ -based catalysts determines their further practical applications. In general, the toxicity of $\text{g-C}_3\text{N}_4$ -based materials is closely associated with their structure, morphology, composition and physicochemical properties such as the surface status, dispersion and hydrophilicity (Chen et al., 2015; Liao et al., 2020). Some investigations have demonstrated that the $\text{g-C}_3\text{N}_4$ -based materials had low toxicity and good biocompatibility, which could meet the requirements of practical applications. For example, Zhang et al. (2013) reported that the ultra-thin $\text{g-C}_3\text{N}_4$ nanosheets possessed nontoxicity and excellent biocompatibility by assessing the viability of HeLa cells after incubation with the $\text{g-C}_3\text{N}_4$ via an MTT (3-(4,5-dimethylthiazol-2-yl)-3,5-diphenyltetrazolium bromide) assay. Even if the concentration of incubated $\text{g-C}_3\text{N}_4$ was as high as $600 \mu\text{g mL}^{-1}$, there was no distinct decrease in cell viability. Feng et al. (2016) found that the up-conversion nanoparticles (UCNP)@ $\text{g-C}_3\text{N}_4$ -polyethylene glycol (PEG) composite itself had no obvious toxicity to HeLa cells. In the study of He et al. (2020), although the short-lived ROS generated by $\text{g-C}_3\text{N}_4$ at a concentration of 50 mg L^{-1} or more under

simulated solar light would exert injury to the hatched zebrafish larvae, the presence of NOM in water could diminish the hazardous effect.

7. Conclusions and perspectives

In conclusion, the $\text{g-C}_3\text{N}_4$ -based catalysts presented excellent catalytic activities in Fenton-based processes, catalytic ozonation and persulfates activation, and could efficiently degrade organic contaminants from water through these AOPs. In Fenton-based processes and catalytic ozonation, the $\bullet\text{OH}$ activated by $\text{g-C}_3\text{N}_4$ -based catalysts was the major reactive species for degrading organic pollutants. While in persulfates activation, the $\text{SO}_4^{\bullet-}$, $\bullet\text{OH}$, $\text{O}_2^{\bullet-}$ and high-valent iron-oxo species were responsible for the degradation of organic pollutants. The effect of water chemistry on catalytic performance indicated that the $\text{g-C}_3\text{N}_4$ -based catalysts could work in a relatively complex water environment. In addition, most of the $\text{g-C}_3\text{N}_4$ -based catalysts exhibited excellent reusability and stability in these AOPs for organic contaminants degradation and showed good biocompatibility. Although some achievements have been made, there are still many challenges to utilize $\text{g-C}_3\text{N}_4$ -based catalysts for the degradation of organic pollutants in water through AOPs beyond photocatalysis. Some points are listed as follows:

1. The catalytic activity and stability of $\text{g-C}_3\text{N}_4$ -based catalysts should be further improved. Despite the high degradation efficiency, there is still much room for improvement in the mineralization rate. Moreover, the stability of some $\text{g-C}_3\text{N}_4$ -based catalysts is unsatisfactory due to the loss of active sites and the leaching of metal species. Thus, it is significant to optimize the synthetic methods of $\text{g-C}_3\text{N}_4$ -based catalysts and develop new types of $\text{g-C}_3\text{N}_4$ -based catalysts with excellent catalytic activity and stability.
2. The oxidation mechanism of organic pollutants and the toxicity of reaction intermediates should be deeply investigated. Theoretical calculation based on DFT can provide a method to reveal the most preferentially attacked sites and potential reaction intermediates of target contaminants. Meanwhile, it is necessary to assess the eco-toxicity or human toxicity of these intermediate products as they are even more toxic than their parent compounds in some cases.
3. The degradation activity test should be performed in the actual wastewater. Normally, there is a huge difference between the composition of simulated wastewater and actual wastewater, which makes the removal efficiency obtained in simulated wastewater less persuasive. Therefore, it is recommended to develop $\text{g-C}_3\text{N}_4$ -based catalysts to target the actual wastewater, which will be beneficial to identify the real challenges in practical applications.
4. The scale of the experiments should be enlarged. To date, most investigations have been executed at the lab-scale using small reactors. To achieve the practical applicability of the $\text{g-C}_3\text{N}_4$ -based catalysts for organic pollutants degradation, more attention should be devoted in the reactor design and scale-up.

Declaration of Competing Interest

The authors declare that they have no known competing financial interests or personal relationships that could have appeared to influence the work reported in this paper.

Acknowledgements

This study was financially supported by the Program for the National Natural Science Foundation of China (51521006, 51879101,

51579098, 51779090, 51709101, 51809090, 51278176, 51378190), the Three Gorges Follow-up Research Project (2017HXXY-05), the National Program for Support of Top-Notch Young Professionals of China (2014), the Program for Changjiang Scholars and Innovative Research Team in University (IRT-13R17), Hunan Provincial Science and Technology Plan Project (2018SK20410, 2017SK2243, 2016RS3026), Postgraduate Scientific Research Innovation Project of Hunan Province (CX20190293), the Natural Science Foundation of Hunan Province, China (grant nos. 2019JJ50077), and the Fundamental Research Funds for the Central Universities (531119200086, 531118010114, 531107050978, 541109060031).

References

- An, S., Zhang, G., Wang, T., Zhang, W., Li, K., Song, C., Miller, J.T., Miao, S., Wang, J., Guo, X., 2018. High-density ultra-small clusters and single-atom Fe sites embedded in graphitic carbon nitride ($\text{g-C}_3\text{N}_4$) for highly efficient catalytic advanced oxidation processes. *ACS Nano* 12 (9), 9441–9450.
- Bai, X., Li, Y., Xie, L., Liu, X., Zhan, S., Hu, W., 2019. A novel Fe-free photo-electro-Fenton-like system for enhanced ciprofloxacin degradation: bifunctional Z-scheme $\text{WO}_3/\text{g-C}_3\text{N}_4$. *Environ. Sci.-Nano* 6 (9), 2850–2862.
- Ball, D.L., Edwards, J.O., 1956. The kinetics and mechanism of the decomposition of caro's acid. *J. Am. Chem. Soc.* 78 (6), 1125–1129.
- Bicalho, H.D.A., Lopez, J.L., Binatti, I., Batista, P.F.R., Ardisson, J.D., Resende, R.R., Lorencon, E., 2017. Facile synthesis of highly dispersed Fe(II) -doped $\text{g-C}_3\text{N}_4$ and its application in Fenton-like catalysis. *Mol. Catal.* 435, 156–165.
- Bokare, A.D., Choi, W., 2014. Review of iron-free Fenton-like systems for activating H_2O_2 in advanced oxidation processes. *J. Hazard. Mater.* 275, 121–135.
- Brown, E.D., Wright, G.D., 2016. Antibacterial drug discovery in the resistance era. *Nature* 529 (7586), 336–343.
- Chen, C., Xie, M., Kong, L., Lu, W., Feng, Z., Zhan, J., 2020a. Mn_3O_4 nanodots loaded $\text{g-C}_3\text{N}_4$ nanosheets for catalytic membrane degradation of organic contaminants. *J. Hazard. Mater.* 390, 122146.
- Chen, C., Zhang, F., Li, C., Lu, J., Cui, S., Liu, H., Li, W., 2017. A magnetic CoFe_2O_4 -CNS nanocomposite as an efficient, recyclable catalyst for peroxymonosulfate activation and pollutant degradation. *RSC Adv.* 7 (87), 55020–55025.
- Chen, S., Huang, D., Zeng, G., Xue, W., Lei, L., Xu, P., Deng, R., Li, J., Cheng, M., 2020b. In-situ synthesis of facet-dependent $\text{BiVO}_4/\text{Ag}_3\text{PO}_4/\text{PANI}$ photocatalyst with enhanced visible-light-induced photocatalytic degradation performance: synergism of interfacial coupling and hole-transfer. *Chem. Eng. J.* 382, 122840.
- Chen, X., Oh, W., Lim, T., 2018. Graphene- and CNTs-based carbocatalysts in persulfates activation: material design and catalytic mechanisms. *Chem. Eng. J.* 354, 941–976.
- Chen, Y., Tan, C., Zhang, H., Wang, L., 2015. Two-dimensional graphene analogues for biomedical applications. *Chem. Soc. Rev.* 44 (9), 2681–2701.
- Cheng, M., Lai, C., Liu, Y., Zeng, G., Huang, D., Zhang, C., Qin, L., Hu, L., Zhou, C., Xiong, W., 2018a. Metal-organic frameworks for highly efficient heterogeneous Fenton-like catalysis. *Coord. Chem. Rev.* 368, 80–92.
- Cheng, M., Zeng, G., Huang, D., Lai, C., Liu, Y., Zhang, C., Wan, J., Hu, L., Zhou, C., Xiong, W., 2018b. Efficient degradation of sulfamethazine in simulated and real wastewater at slightly basic pH values using Co-SAM-SCS/ H_2O_2 Fenton-like system. *Water Res.* 138, 7–18.
- Deng, R., Luo, H., Huang, D., Zhang, C., 2020. Biochar-mediated Fenton-like reaction for the degradation of sulfamethazine: role of environmentally persistent free radicals. *Chemosphere* 255, 126975.
- Ding, F., Yang, D., Tong, Z., Nan, Y., Wang, Y., Zou, X., Jiang, Z., 2017. Graphitic carbon nitride-based nanocomposites as visible-light driven photocatalysts for environmental purification. *Environ. Sci.-Nano* 4 (7), 1455–1469.
- Ding, Q., Lam, F.L.Y., Hu, X., 2019. Complete degradation of ciprofloxacin over $\text{g-C}_3\text{N}_4$ -iron oxide composite via heterogeneous dark Fenton reaction. *J. Environ. Manage.* 244, 23–32.
- Dong, H., Wei, M., Li, J., Fang, J., Gao, L., Li, X., Xu, A., 2016. Catalytic performance of supported $\text{g-C}_3\text{N}_4$ on $\text{MCM}-41$ in organic dye degradation with peroxymonosulfate. *RSC Adv.* 6 (75), 70747–70755.
- Duan, X., Sun, H., Kang, J., Wang, Y., Indrawirawan, S., Wang, S., 2015. Insights into heterogeneous catalysis of persulfate activation on dimensional-structured nanocarbons. *ACS Catal.* 5 (8), 4629–4636.
- Esplugas, S., Bila, D.M., Krause, L.G.T., Dezotti, M., 2007. Ozonation and advanced oxidation technologies to remove endocrine disrupting chemicals (EDCs) and pharmaceuticals and personal care products (PPCPs) in water effluents. *J. Hazard. Mater.* 149 (3), 631–642.
- Fan, J., Qin, H., Jiang, S., 2019. Mn-doped $\text{g-C}_3\text{N}_4$ composite to activate peroxymonosulfate for acetaminophen degradation: the role of superoxide anion and singlet oxygen. *Chem. Eng. J.* 359, 723–732.
- Fang, G., Dionysiou, D.D., Al-Abed, S.R., Zhou, D., 2013. Superoxide radical driving the activation of persulfate by magnetite nanoparticles: implications for the degradation of PCBs. *Appl. Catal. B: Environ.* 129, 325–332.
- Fang, L., Liu, Z., Zhou, C., Guo, Y., Feng, Y., Yang, M., 2019. Degradation mechanism of methylene blue by H_2O_2 and synthesized carbon nanodots/graphitic carbon nitride/ Fe(II) composite. *J. Phys. Chem. C* 123 (44), 26921–26931.
- Feng, L., He, F., Liu, B., Yang, G., Gai, S., Yang, P., Li, C., Dai, Y., Lv, R., Lin, J., 2016. $\text{g-C}_3\text{N}_4$ coated upconversion nanoparticles for 808nm near-infrared light triggered phototherapy and multiple imaging. *Chem. Mater.* 28 (21), 7946.

- Feng, Y., Li, H., Wu, D., Liao, C., Fan, Y., Lee, P., Shih, K., 2018a. Supported palladium nanoparticles as highly efficient catalysts for radical production: support-dependent synergistic effects. *Chemosphere* 207, 27–32.
- Feng, Y., Liao, C., Kong, L., Wu, D., Liu, Y., Lee, P., Shih, K., 2018b. Facile synthesis of highly reactive and stable Fe-doped g-C₃N₄ composites for peroxymonosulfate activation: a novel nonradical oxidation process. *J. Hazard. Mater.* 354, 63–71.
- Gao, H., Yang, H., Xu, J., Zhang, S., Li, J., 2018a. Strongly coupled g-C₃N₄ nanosheets-Co₃O₄ quantum dots as 2D/0D heterostructure composite for peroxymonosulfate activation. *Small* 14 (31), 1801353.
- Gao, Y., Li, S., Li, Y., Yao, L., Zhang, H., 2017. Accelerated photocatalytic degradation of organic pollutant over metal-organic framework MIL-53(Fe) under visible LED light mediated by persulfate. *Appl. Catal. B: Environ.* 202, 165–174.
- Gao, Y., Zhu, Y., Lyu, L., Zeng, Q., Xing, X., Hu, C., 2018b. Electronic structure modulation of graphitic carbon nitride by oxygen doping for enhanced catalytic degradation of organic pollutants through peroxymonosulfate activation. *Environ. Sci. Technol.* 52 (24), 14371–14380.
- Ge, L., Peng, Z., Wang, W., Tan, F., Wang, X., Su, B., Qiao, X., Wong, P.K., 2018. g-C₃N₄/MgO nanosheets: light-independent, metal-poisoning-free catalysts for the activation of hydrogen peroxide to degrade organics. *J. Mater. Chem. A* 6 (34), 16421–16429.
- Gholami, P., Dipazhoh, L., Khataee, A., Hassani, A., Bhatnagar, A., 2020a. Facile hydrothermal synthesis of novel Fe-Cu layered double hydroxide/biochar nanocomposite with enhanced sonocatalytic activity for degradation of cefazolin sodium. *J. Hazard. Mater.* 381, 120742.
- Gholami, P., Khataee, A., Bhatnagar, A., 2020b. Environmentally superior cleaning of diatom frustules using sono-Fenton process: facile fabrication of nanoporous silica with homogeneous morphology and controlled size. *Ultrasound. Sonochem.* 64, 105044.
- Guan, C., Jiang, J., Pang, S., Chen, X., Webster, R.D., Lim, T., 2020. Facile synthesis of pure g-C₃N₄ materials for peroxymonosulfate activation to degrade bisphenol A: effects of precursors and annealing ambience on catalytic oxidation. *Chem. Eng. J.* 387, 123726.
- Guo, F., Lu, J., Liu, Q., Zhang, P., Zhang, A., Cai, Y., Wang, Q., 2018. Degradation of Acid Orange 7 by peroxymonosulfate activated with the recyclable nanocomposites of g-C₃N₄ modified magnetic carbon. *Chemosphere* 205, 297–307.
- Guo, H., Niu, C., Feng, C., Liang, C., Zhang, L., Wen, X., Yang, Y., Liu, H., Li, L., Lin, L., 2020a. Steering exciton dissociation and charge migration in green synthetic oxygen-substituted ultrathin porous graphitic carbon nitride for boosted photocatalytic reactive oxygen species generation. *Chem. Eng. J.* 385, 123919.
- Guo, H., Niu, H., Liang, C., Niu, C., Liu, Y., Tang, N., Yang, Y., Liu, H., Yang, Y., Wang, W., 2020b. Few-layer graphitic carbon nitride nanosheet with controllable functionalization as an effective metal-free activator for peroxymonosulfate photocatalytic activation: role of the energy band bending. *Chem. Eng. J.* 401, 126072.
- Guo, Z., Xie, Y., Xiao, J., Zhao, Z., Wang, Y., Xu, Z., Zhang, Y., Yin, L., Cao, H., Gong, J., 2019. Single-atom Mn-N₄ site-catalyzed perozone reaction for the efficient production of hydroxyl radicals in an acidic solution. *J. Am. Chem. Soc.* 141 (30), 12005–12010.
- Hao, Q., Jia, G., Wei, W., Vinu, A., Wang, Y., Arandiyani, H., Ni, B., 2020. Graphitic carbon nitride with different dimensionalities for energy and environmental applications. *Nano Res.* 13 (1), 18–37.
- He, D., Niu, H., He, S., Mao, L., Cai, Y., Liang, Y., 2019a. Strengthened fenton degradation of phenol catalyzed by core/shell Fe-Pd@C nanocomposites derived from mechanochemically synthesized Fe-Metal organic frameworks. *Water Res.* 162, 151–160.
- He, D., Zhang, C., Zeng, G., Yang, Y., Huang, D., Wang, L., Wang, H., 2019b. A multi-functional platform by controlling of carbon nitride in the core-shell structure: from design to construction, and catalysis applications. *Appl. Catal. B: Environ.* 258, 117957.
- He, Y., Peng, G., Jiang, Y., Zhao, M., Wang, X., Chen, M., Lin, S., 2020. Environmental hazard potential of nano-photocatalysts determined by nano-bio interactions and exposure conditions. *Small* 16, 1907690.
- Herney-Ramirez, J., Vicente, M.A., Madeira, L.M., 2010. Heterogeneous photo-Fenton oxidation with pillared clay-based catalysts for wastewater treatment: a review. *Appl. Catal. B: Environ.* 98 (1–2), 10–26.
- Huang, D., Li, Z., Zeng, G., Zhou, C., Xue, W., Gong, X., Yan, X., Chen, S., Wang, W., Cheng, M., 2019a. Megamer in photocatalytic field: 2D g-C₃N₄ nanosheets serve as support of 0D nanomaterials for improving photocatalytic performance. *Appl. Catal. B: Environ.* 240, 153–173.
- Huang, D., Luo, H., Zhang, C., Zeng, G., Lai, C., Cheng, M., Wang, R., Deng, R., Xue, W., Gong, X., 2019b. Nonnegligible role of biomass types and its compositions on the formation of persistent free radicals in biochar: insight into the influences on Fenton-like process. *Chem. Eng. J.* 361, 353–363.
- Hubner, U., Von Gunten, U., Jekel, M., 2015. Evaluation of the persistence of transformation products from ozonation of trace organic compounds - a critical review. *Water Res.* 68, 150–170.
- Jia, M., Yang, Z., Xu, H., Song, P., Xiong, W., Cao, J., Zhang, Y., Xiang, Y., Hu, J., Zhou, C., 2020. Integrating N and F co-doped TiO₂ nanotubes with ZIF-8 as photoelectrode for enhanced photo-electrocatalytic degradation of sulfamethazine. *Chem. Eng. J.* 388, 124388.
- Khataee, A., Gholami, P., Vahid, B., 2017. Catalytic performance of hematite nanostructures prepared by N₂ glow discharge plasma in heterogeneous Fenton-like process for acid red 17 degradation. *J. Ind. Eng. Chem.* 50, 86–95.
- Khataee, A., Gholami, P., Vahid, B., Joo, S.W., 2016. Heterogeneous sono-Fenton process using pyrite nanorods prepared by non-thermal plasma for degradation of an anthraquinone dye. *Ultrasound. Sonochem.* 32, 357–370.
- Klavarioti, M., Mantzavinos, D., Kassinos, D., 2009. Removal of residual pharmaceuticals from aqueous systems by advanced oxidation processes. *Environ. Int.* 35 (2), 402–417.
- Lan, H., Wang, F., Lan, M., An, X., Liu, H., Qu, J., 2019. Hydrogen-bond-mediated self-assembly of carbon-nitride-based photo-Fenton-like membranes for wastewater treatment. *Environ. Sci. Technol.* 53 (12), 6981–6988.
- Lefebvre, O., Moletta, R., 2006. Treatment of organic pollution in industrial saline wastewater: a literature review. *Water Res.* 40 (20), 3671–3682.
- Lei, L., Huang, D., Zhang, C., Deng, R., Chen, S., Li, Z., 2020a. F dopants triggered active sites in bifunctional cobalt sulfide/nickel foam toward electrocatalytic overall water splitting in neutral and alkaline media: experiments and theoretical calculations. *J. Catal.* 385, 129–139.
- Lei, L., Huang, D., Zhou, C., Chen, S., Yan, X., Li, Z., Wang, W., 2020b. Demystifying the active roles of NiFe-based oxides/(oxy) hydroxides for electrochemical water splitting under alkaline conditions. *Coord. Chem. Rev.* 408, 213177.
- Li, H., Shan, C., Pan, B., 2018. Fe(III)-doped g-C₃N₄ mediated peroxymonosulfate activation for selective degradation of phenolic compounds via high-valent iron-oxo species. *Environ. Sci. Technol.* 52 (4), 2197–2205.
- Li, H., Shan, C., Pan, B., 2019a. Development of Fe-doped g-C₃N₄/graphite mediated peroxymonosulfate activation for degradation of aromatic pollutants via non-radical pathway. *Sci. Total Environ.* 675, 62–72.
- Li, J., Fang, J., Gao, L., Zhang, J., Ruan, X., Xu, A., Li, X., 2017. Graphitic carbon nitride induced activity enhancement of OMS-2 catalyst for pollutants degradation with peroxymonosulfate. *Appl. Surf. Sci.* 402, 352–359.
- Li, J., Li, X., Han, J., Meng, F., Jiang, J., Li, J., Xu, C., Li, Y., 2019b. Mesoporous bimetallic Fe/Co as highly active heterogeneous Fenton catalyst for the degradation of tetracycline hydrochlorides. *Sci. Rep.* 9 (1), 15820.
- Li, J., Pham, A.N., Dai, R., Wang, Z., Waite, T.D., 2020a. Recent advances in Cu-Fenton systems for the treatment of industrial wastewaters: role of Cu complexes and Cu composites. *J. Hazard. Mater.* 392, 122261.
- Li, L., Lai, C., Huang, F., Cheng, M., Zeng, G., Huang, D., Li, B., Liu, S., Zhang, M., Qin, L., 2019c. Degradation of naphthalene with magnetic bio-char activate hydrogen peroxide: synergism of bio-char and Fe-Mn binary oxides. *Water Res.* 160, 238–248.
- Li, R., Cai, M., Xie, Z., Zhang, Q., Zeng, Y., Liu, H., Liu, G., Lv, W., 2019d. Construction of heterostructured CuFe₂O₄/g-C₃N₄ nanocomposite as an efficient visible light photocatalyst with peroxydisulfate for the organic oxidation. *Appl. Catal. B: Environ.* 244, 974–982.
- Li, W., Cao, J., Xiong, W., Yang, Z., Sun, S., Jia, M., Xu, Z., 2020b. In-situ growing of metal-organic frameworks on three-dimensional iron network as an efficient adsorbent for antibiotics removal. *Chem. Eng. J.* 392, 124844.
- Li, X., Wang, Y., Zhao, J., Wang, H., Wang, B., Huang, J., Deng, S., Yu, G., 2015. Electro-peroxone treatment of the antidepressant venlafaxine: operational parameters and mechanism. *J. Hazard. Mater.* 300, 298–306.
- Li, X., Zeng, Z., Zeng, G., Wang, D., Xiao, R., Wang, Y., Zhou, C., Yi, H., Ye, S., Yang, Y., 2020c. A “bottle-around-ship” like method synthesized yolk-shell Ag₃PO₄@MIL-53(Fe) Z-scheme photocatalysts for enhanced tetracycline removal. *J. Colloid Interface Sci.* 561, 501–511.
- Li, Y., Kong, T., Shen, S., 2019e. Artificial photosynthesis with polymeric carbon nitride: when meeting metal nanoparticles, single atoms, and molecular complexes. *Small* 15 (32), 1900772.
- Li, Y., Li, J., Pan, Y., Xiong, Z., Yao, G., Xie, R., Lai, B., 2020d. Peroxymonosulfate activation on FeCo₂S₄ modified g-C₃N₄ (FeCo₂S₄-CN): mechanism of singlet oxygen evolution for nonradical efficient degradation of sulfamethoxazole. *Chem. Eng. J.* 384, 123361.
- Li, Y., Ouyang, S., Xu, H., Wang, X., Bi, Y., Zhang, Y., Ye, J., 2016. Constructing solid-gas-interfacial fenton reaction over alkalinized-C₃N₄ photocatalyst to achieve apparent quantum yield of 49% at 420nm. *J. Am. Chem. Soc.* 138 (40), 13289–13297.
- Liao, G., He, F., Li, Q., Zhong, L., Zhao, R., Che, H., Gao, H., Fang, B., 2020. Emerging graphitic carbon nitride-based materials for biomedical applications. *Prog. Mater Sci.* 112, 100666.
- Lin, K.A., Yang, M., Zhang, Z., Wiafedzi, T., Lin, Y., 2018a. Prussian Blue analogue supported on sulfur-doped carbon nitride as an enhanced heterogeneous catalyst for activating peroxymonosulfate. *J. Colloid Interface Sci.* 529, 161–170.
- Lin, K.A., Zhang, Z., Wiafedzi, T., 2018b. Sulfur-doped carbon nitride as a non-metal heterogeneous catalyst for sulfate radical-based advanced oxidation processes in the absence of light irradiation. *J. Water Process Eng.* 24, 83–89.
- Lin, Y., Liu, H., Yang, C., Wu, X., Du, C., Jiang, L., Zhong, Y., 2020. Gama-graphyne as photogenerated electrons transfer layer enhances photocatalytic performance of silver phosphate. *Appl. Catal. B: Environ.* 264, 118479.
- Liu, J., Li, J., He, S., Sun, L., Yuan, X., Xia, D., 2020a. Heterogeneous catalytic ozonation of oxalic acid with an effective catalyst based on copper oxide modified g-C₃N₄. *Sep. Purif. Technol.* 234, 116120.
- Liu, J., Wong, M.H., 2013. Pharmaceuticals and personal care products (PPCPs): a review on environmental contamination in China. *Environ. Int.* 59, 208–224.
- Liu, S., Lai, C., Li, B., Zhang, C., Zhang, M., Huang, D., Qin, L., Yi, H., Liu, X., Huang, F., 2020b. Role of radical and non-radical pathway in activating persulfate for degradation of p-nitrophenol by sulfur-doped ordered mesoporous carbon. *Chem. Eng. J.* 384, 123304.
- Liu, Y., Cheng, M., Liu, Z., Zeng, G., Zhong, H., Chen, M., Zhou, C., Xiong, W., Shao, B., Song, B., 2019. Heterogeneous Fenton-like catalyst for treatment of rhamnolipid-solubilized hexadecane wastewater. *Chemosphere* 236, 124387.
- Loeb, S., Alvarez, P.J.J., Brame, J., Cates, E.L., Choi, W., Crittenden, J.C., Dionysiou, D.D., Li, Q., Lipuma, G., Quan, X., 2019. The technology horizon for photocatalytic water treatment: sunrise or sunset? *Environ. Sci. Technol.* 53 (6), 2937–2947.

- Lu, K., Yang, F., Lin, W., Zhou, S., Xi, T., Song, C., Kong, Y., 2018. Stabilized pony-sized-CuFe₂O₄/carbon nitride porous composites with boosting Fenton-like oxidation activity. *ChemistrySelect* 3, 4207–4216.
- Lu, X., Zhao, J., Wang, Q., Wang, D., Xu, H., Ma, J., Qiu, W., Hu, T., 2019. Sonolytic degradation of bisphenol S: effect of dissolved oxygen and peroxydisulfate, oxidation products and acute toxicity. *Water Res.* 165, 114969.
- Luo, L., Zhang, A., Janik, M.J., Song, C., Guo, X., 2016. Mesoporous graphitic carbon nitride functionalized iron oxides for promoting phenol oxidation activity. *RSC Adv.* 6 (94), 91960–91967.
- Lyu, L., Yan, D., Yu, G., Cao, W., Hu, C., 2018. Efficient destruction of pollutants in water by a dual-reaction-center Fenton-like process over carbon nitride compounds-complexed Cu(II)-CuAlO₂. *Environ. Sci. Technol.* 52 (7), 4294–4304.
- Lyu, L., Zhang, L., He, G., He, H., Hu, C., 2017. Selective H₂O₂ conversion to hydroxyl radicals in the electron-rich area of hydroxylated C-g-C₃N₄/CuCo-Al₂O₃. *J. Mater. Chem. A* 5 (15), 7153–7164.
- Lyu, L., Zhang, L., Wang, Q., Nie, Y., Hu, C., 2015. Enhanced fenton catalytic efficiency of γ -Cu-Al₂O₃ by σ -Cu²⁺-ligand complexes from aromatic pollutant degradation. *Environ. Sci. Technol.* 49 (14), 8639–8647.
- Ma, J., Huang, Z., Xi, H., Wen, Y., 2019a. Magnetic Fe-doping g-C₃N₄/graphite: the effect of supporters and the performance in Fenton-like reactions. *Desalin. Water Treat.* 142, 371–380.
- Ma, J., Jia, N., Shen, C., Liu, W., Wen, Y., 2019b. Stable cuprous active sites in Cu⁺-graphitic carbon nitride: structure analysis and performance in Fenton-like reactions. *J. Hazard. Mater.* 378, 120782.
- Ma, J., Yang, Q., Wen, Y., Liu, W., 2017. Fe-g-C₃N₄/graphitized mesoporous carbon composite as an effective Fenton-like catalyst in a wide pH range. *Appl. Catal. B: Environ.* 201, 232–240.
- Mamba, G., Mishra, A.K., 2016. Graphitic carbon nitride (g-C₃N₄) nanocomposites: a new and exciting generation of visible light driven photocatalysts for environmental pollution remediation. *Appl. Catal. B: Environ.* 198, 347–377.
- Melchionna, M., Fornasiero, P., 2020. Updates on the Roadmap for Photocatalysis. *ACS Catal.* 10 (10), 5493–5501.
- Miklos, D., Remy, C., Jekel, M., Linden, K.G., Drewes, J.E., Hubner, U., 2018. Evaluation of advanced oxidation processes for water and wastewater treatment – a critical review. *Water Res.* 139, 118–131.
- Muir, D.C.G., Howard, P.H., 2006. Are there other persistent organic pollutants? A challenge for environmental chemists. *Environ. Sci. Technol.* 40 (23), 7157–7166.
- Nawrocki, J., Kasprzykhordern, B., 2010. The efficiency and mechanisms of catalytic ozonation. *Appl. Catal. B: Environ.* 99 (1), 27–42.
- Nguyen, T.B., Doong, R., Huang, C.P., Chen, C., Dong, C., 2019. Activation of persulfate by CoO nanoparticles loaded on 3D mesoporous carbon nitride (CoO@meso-CN) for the degradation of methylene blue (MB). *Sci. Total Environ.* 675, 531–541.
- Nosaka, Y., Nosaka, A.Y., 2017. Generation and detection of reactive oxygen species in photocatalysis. *Chem. Rev.* 117 (17), 11302–11336.
- Oh, W., Chang, V.W.C., Hu, Z., Goei, R., Lim, T., 2017. Enhancing the catalytic activity of g-C₃N₄ through Me doping (Me = Cu, Co and Fe) for selective sulfathiazole degradation via redox-based advanced oxidation process. *Chem. Eng. J.* 323, 260–269.
- Ong, W., Tan, L., Ng, Y.H., Yong, S.T., Chai, S., 2016. Graphitic carbon nitride (g-C₃N₄)-based photocatalysts for artificial photosynthesis and environmental remediation: are we a step closer to achieving sustainability? *Chem. Rev.* 116 (12), 7159–7329.
- Oturán, M.A., Aaron, J., 2014. Advanced oxidation processes in water/wastewater treatment: principles and applications. A review. *Crit. Rev. Environ. Sci. Technol.* 44 (23), 2577–2641.
- Pi, Y., Gao, H., Cao, Y., Cao, R., Wang, Y., Sun, J., 2020. Cobalt ferrite supported on carbon nitride matrix prepared using waste battery materials as a peroxymonosulfate activator for the degradation of levofloxacin hydrochloride. *Chem. Eng. J.* 379, 122377.
- Pignatello, J.J., Oliveros, E., Mackay, A.A., 2006. Advanced oxidation processes for organic contaminant destruction based on the Fenton reaction and related chemistry. *Crit. Rev. Environ. Sci. Technol.* 36 (1), 1–84.
- Qin, F., Peng, Y., Song, G., Fang, Q., Wang, R., Zhang, C., Zeng, G., Huang, D., Lai, C., Zhou, Y., 2020. Degradation of sulfamethazine by biochar-supported bimetallic oxide/persulfate system in natural water: performance and reaction mechanism. *J. Hazard. Mater.* 122816.
- Qin, Q., Gao, X., Wu, X., Liu, Y., 2019. NaBH₄-treated cobalt-doped g-C₃N₄ for enhanced activation of peroxymonosulfate. *Mater. Lett.* 256, 126623.
- Ren, Y., Shi, M., Zhang, W., Dionysiou, D.D., Lu, J., Shan, C., Zhang, Y., Lv, L., Pan, B., 2020. Enhancing the Fenton-like Catalytic Activity of nFe₂O₃ by MIL-53(Cu) support: a mechanistic investigation. *Environ. Sci. Technol.* 54 (8), 5258–5267.
- Sein, M.M., Zedda, M., Tuerk, J., Schmidt, T.C., Golloch, A., Von Sonntag, C., 2008. Oxidation of diclofenac with ozone in aqueous solution. *Environ. Sci. Technol.* 42 (17), 6656–6662.
- Song, B., Xu, P., Zeng, G., Gong, J., Wang, X., Yan, J., Wang, S., Zhang, P., Cao, W., Ye, S., 2018. Modeling the transport of sodium dodecyl benzene sulfonate in riverine sediment in the presence of multi-walled carbon nanotubes. *Water Res.* 129, 20–28.
- Song, B., Zeng, Z., Zeng, G., Gong, J., Xiao, R., Ye, S., Chen, M., Lai, C., Xu, P., Tang, X., 2019a. Powerful combination of g-C₃N₄ and LDHs for enhanced photocatalytic performance: a review of strategy, synthesis, and applications. *Adv. Colloid Interface Sci.*, 101999.
- Song, Z., Zhang, Y., Liu, C., Xu, B., Qi, F., Yuan, D., Pu, S., 2019b. Insight into •OH and •O₂^{•-} formation in heterogeneous catalytic ozonation by delocalized electrons and surface oxygen-containing functional groups in layered-structure nanocarbons. *Chem. Eng. J.* 357, 655–666.
- Soon, A.N., Hameed, B., 2011. Heterogeneous catalytic treatment of synthetic dyes in aqueous media using Fenton and photo-assisted Fenton process. *Desalination* 269 (1–3), 1–16.
- Tan, T., Zeng, Z., Zeng, G., Gong, J., Xiao, R., Zhang, P., Song, B., Tang, W., Ren, X., 2020. Electrochemically enhanced simultaneous degradation of sulfamethoxazole, ciprofloxacin and amoxicillin from aqueous solution by multi-walled carbon nanotube filter. *Sep. Purif. Technol.* 235, 116167.
- Teixeira, I.F., Barbosa, E.C.M., Tsang, S.C., Camargo, P.H.C., 2018. Carbon nitrides and metal nanoparticles: from controlled synthesis to design principles for improved photocatalysis. *Chem. Soc. Rev.* 47 (20), 7783–7817.
- Tian, S., Zhang, C., Huang, D., Wang, R., Zeng, G., Yan, M., Xiong, W., Zhou, C., Cheng, M., Xue, W., 2020. Recent progress in sustainable technologies for adsorptive and reactive removal of sulfonamides. *Chem. Eng. J.* 389, 123423.
- Wang, D., Saleh, N.B., Sun, W., Park, C.M., Shen, C., Aich, N., Peijnenburg, W.J.G.M., Zhang, W., Jin, Y., Su, C., 2019a. Next-generation multifunctional carbon-metal nanohybrids for energy and environmental applications. *Environ. Sci. Technol.* 53 (13), 7265–7287.
- Wang, J., Bai, Z., 2017. Fe-based catalysts for heterogeneous catalytic ozonation of emerging contaminants in water and wastewater. *Chem. Eng. J.* 312, 79–98.
- Wang, J., Chen, H., 2020. Catalytic ozonation for water and wastewater treatment: recent advances and perspective. *Sci. Total Environ.* 704, 135249.
- Wang, J., Quan, X., Chen, S., Yu, H., Liu, G., 2019b. Enhanced catalytic ozonation by highly dispersed CeO₂ on carbon nanotubes for mineralization of organic pollutants. *J. Hazard. Mater.* 368, 621–629.
- Wang, J., Wang, S., 2018. Activation of persulfate (PS) and peroxymonosulfate (PMS) and application for the degradation of emerging contaminants. *Chem. Eng. J.* 334, 1502–1517.
- Wang, J., Xu, L.J., 2012. Advanced oxidation processes for wastewater treatment: formation of hydroxyl radical and application. *Crit. Rev. Environ. Sci. Technol.* 42 (3), 251–325.
- Wang, J., Yue, M., Han, Y., Xu, X., Yue, Q., Xu, S., 2019c. Highly-efficient degradation of triclosan attributed to peroxymonosulfate activation by heterogeneous catalyst g-C₃N₄/MnFe₂O₄. *Chem. Eng. J.* 123554.
- Wang, L., Zhang, Q., Chen, B., Bu, Y., Chen, Y., Ma, J., Rosario-Ortiz, F.L., Zhu, R., 2020a. Some issues limiting photo (cata) lysis application in water pollutant control: a critical review from chemistry perspectives. *Water Res.* 174, 115605.
- Wang, S., Liu, Y., Wang, J., 2020b. Iron and sulfur co-doped graphite carbon nitride (FeO_x/S-g-C₃N₄) for activating peroxymonosulfate to enhance sulfamethoxazole degradation. *Chem. Eng. J.* 382, 122836.
- Wang, W., Niu, Q., Zeng, G., Zhang, C., Huang, D., Shao, B., Zhou, C., Yang, Y., Liu, Y., Guo, H., 2020c. 1D porous tubular g-C₃N₄ capture black phosphorus quantum dots as 1D/0D metal-free photocatalysts for oxytetracycline hydrochloride degradation and hexavalent chromium reduction. *Appl. Catal. B: Environ.* 273, 119051.
- Wang, W., Wang, H., Li, G., Wong, P.K., An, T., 2020d. Visible light activation of persulfate by magnetic hydrochar for bacterial inactivation: efficiency, recyclability and mechanisms. *Water Res.* 176, 115746.
- Wang, W., Xu, P., Chen, M., Zeng, G., Zhang, C., Zhou, C., Yang, Y., Huang, D., Lai, C., Cheng, M., 2018. Alkali metal-assisted synthesis of graphite carbon nitride with tunable band-gap for enhanced visible-light-driven photocatalytic performance. *ACS Sustain. Chem. Eng.* 6 (11), 15503–15516.
- Wang, W., Zeng, Z., Zeng, G., Zhang, C., Xiao, R., Zhou, C., Xiong, W., Yang, Y., Lei, L., Liu, Y., 2019d. Sulfur doped carbon quantum dots loaded hollow tubular g-C₃N₄ as novel photocatalyst for destruction of Escherichia coli and tetracycline degradation under visible light. *Chem. Eng. J.* 378, 122132.
- Wang, X., Nan, Z., 2020. Highly efficient Fenton-like catalyst Fe-g-C₃N₄ porous nanosheets formation and catalytic mechanism. *Sep. Purif. Technol.* 233, 116023.
- Wang, Y., Cao, D., Liu, M., Zhao, X., 2017. Insights into heterogeneous catalytic activation of peroxymonosulfate by Pd/g-C₃N₄: the role of superoxide radical and singlet oxygen. *Catal. Commun.* 102, 85–88.
- Wang, Z., Wang, H., Zeng, Z., Zeng, G., Xu, P., Xiao, R., Huang, D., Chen, X., He, L., Zhou, C., 2020e. Metal-organic Frameworks derived Bi₂O₂CO₃/porous carbon nitride: a nanosized Z-scheme systems with enhanced photocatalytic activity. *Appl. Catal. B: Environ.* 267, 118700.
- Wei, M., Gao, L., Li, J., Fang, J., Cai, W., Li, X., Xu, A., 2016. Activation of peroxymonosulfate by graphitic carbon nitride loaded on activated carbon for organic pollutants degradation. *J. Hazard. Mater.* 316, 60–68.
- Wu, S., Liu, H., Yang, C., Li, X., Lin, Y., Yin, K., Sun, J., Teng, Q., Du, C., Zhong, Y., 2019. High-performance porous carbon catalysts doped by iron and nitrogen for degradation of bisphenol F via peroxymonosulfate activation. *Chem. Eng. J.* 392, 123683.
- Xi, J., Xia, H., Ning, X., Zhang, Z., Liu, J., Mu, Z., Zhang, S., Du, P., Lu, X., 2019. Carbon-intercalated 0D/2D hybrid of hematite quantum dots/graphitic carbon nitride nanosheets as superior catalyst for advanced oxidation. *Small* 15 (43), 1902744.
- Xiao, J., Han, Q., Xie, Y., Yang, J., Su, Q., Chen, Y., Cao, H., 2017. Is C₃N₄ chemically stable toward reactive oxygen species in sunlight-driven water treatment? *Environ. Sci. Technol.* 51 (22), 13380–13387.
- Xiao, S., Cheng, M., Zhong, H., Liu, Z., Liu, Y., Yang, X., Liang, Q., 2020. Iron-mediated activation of persulfate and peroxymonosulfate in both homogeneous and heterogeneous ways: a review. *Chem. Eng. J.* 384, 123265.
- Xie, M., Tang, J., Kong, L., Lu, W., Natarajan, V., Zhu, F., Zhan, J., 2019. Cobalt doped g-C₃N₄ activation of peroxymonosulfate for monochlorophenols degradation. *Chem. Eng. J.* 360, 1213–1222.
- Xie, Y., Peng, S., Feng, Y., Wu, D., 2020. Enhanced mineralization of oxalate by highly

- active and stable Ce(III)-doped g-C₃N₄ catalyzed ozonation. Chemosphere 239, 124612.
- Xiong, W., Zeng, Z., Zeng, G., Yang, Z., Xiao, R., Li, X., Cao, J., Zhou, C., Chen, H., Jia, M., 2019. Metal-organic frameworks derived magnetic carbon- α Fe/Fe₃C composites as a highly effective adsorbent for tetracycline removal from aqueous solution. Chem. Eng. J. 374, 91–99.
- Xu, H., Ma, R., Zhu, Y., Du, M., Zhang, H., Jiao, Z., 2020. A systematic study of the antimicrobial mechanisms of cold atmospheric-pressure plasma for water disinfection. Sci. Total Environ. 703, 134965.
- Xu, L., Wang, J., 2012. Fenton-like degradation of 2, 4-dichlorophenol using Fe₃O₄ magnetic nanoparticles. Appl. Catal. B: Environ. 123, 117–126.
- Xu, S., Zhu, H., Cao, W., Wen, Z., Wang, J., Francoisxavier, C.P., Wintgens, T., 2018. Cu-Al₂O₃-g-C₃N₄ and Cu-Al₂O₃-C-dots with dual-reaction centres for simultaneous enhancement of Fenton-like catalytic activity and selective H₂O₂ conversion to hydroxyl radicals. Appl. Catal. B: Environ. 234, 223–233.
- Yang, M., Zhang, Z., Lin, K.A., 2019a. One-step fabrication of cobalt-embedded carbon nitride as a magnetic and efficient heterogeneous catalyst for activating oxone to degrade pollutants in water. Sep. Purif. Technol. 210, 1–9.
- Yang, Q., Ma, Y., Chen, F., Yao, F., Sun, J., Wang, S., Yi, K., Hou, L., Li, X., Wang, D., 2019b. Recent advances in photo-activated sulfate radical-advanced oxidation process (SR-AOP) for refractory organic pollutants removal in water. Chem. Eng. J. 378, 122149.
- Yang, Y., Zeng, G., Huang, D., Zhang, C., He, D., Zhou, C., Wang, W., Xiong, W., Li, X., Li, B., 2020a. Molecular engineering of polymeric carbon nitride for highly efficient photocatalytic oxytetracycline degradation and H₂O₂ production. Appl. Catal. B: Environ. 272, 118970.
- Yang, Y., Zeng, G., Huang, D., Zhang, C., He, D., Zhou, C., Wang, W., Xiong, W., Song, B., Yi, H., 2020b. In situ grown single-atom cobalt on polymeric carbon nitride with bidentate ligand for efficient photocatalytic degradation of refractory antibiotics. Small, 2001634.
- Yang, Y., Zeng, Z., Zeng, G., Huang, D., Xiao, R., Zhang, C., Zhou, C., Xiong, W., Wang, W., Cheng, M., 2019c. Ti₃C₂ Mxene/porous g-C₃N₄ interfacial Schottky junction for boosting spatial charge separation in photocatalytic H₂O₂ production. Appl. Catal. B: Environ. 258, 117956.
- Yang, Y., Zeng, Z., Zhang, C., Huang, D., Zeng, G., Xiao, R., Lai, C., Zhou, C., Guo, H., Xue, W., 2018a. Construction of iodine vacancy-rich BiOI/Ag@AgI Z-scheme heterojunction photocatalysts for visible-light-driven tetracycline degradation: transformation pathways and mechanism insight. Chem. Eng. J. 349, 808–821.
- Yang, Y., Zhang, C., Huang, D., Zeng, G., Huang, J., Lai, C., Zhou, C., Wang, W., Guo, H., Xue, W., 2019d. Boron nitride quantum dots decorated ultrathin porous g-C₃N₄: intensified exciton dissociation and charge transfer for promoting visible-light-driven molecular oxygen activation. Appl. Catal. B: Environ. 245, 87–99.
- Yang, Y., Zhang, C., Lai, C., Zeng, G., Huang, D., Cheng, M., Wang, J., Chen, F., Zhou, C., Xiong, W., 2018b. BioX (X= Cl, Br, I) photocatalytic nanomaterials: applications for fuels and environmental management. Adv. Colloid Interface Sci. 254, 76–93.
- Yang, Z., Zhang, C., Zeng, G., Tan, X., Wang, H., Huang, D., Yang, K., Wei, J., Ma, C., Nie, K., 2020c. Design and engineering of layered double hydroxide based catalysts for water depollution by advanced oxidation processes: a review. J. Mater. Chem. A 8 (8), 4141–4173.
- Yao, Y., Hu, Y., Hu, H., Chen, L., Yu, M., Gao, M., Wang, S., 2019. Metal-free catalysts of graphitic carbon nitride-covalent organic frameworks for efficient pollutant destruction in water. J. Colloid Interface Sci. 554, 376–387.
- Ye, S., Yan, M., Tan, X., Liang, J., Zeng, G., Wu, H., Song, B., Zhou, C., Yang, Y., Wang, H., 2019a. Facile assembled biochar-based nanocomposite with improved graphitization for efficient photocatalytic activity driven by visible light. Appl. Catal. B: Environ. 250, 78–88.
- Ye, S., Zeng, G., Wu, H., Liang, J., Zhang, C., Dai, J., Xiong, W., Song, B., Wu, S., Yu, J., 2019b. The effects of activated biochar addition on remediation efficiency of co-composting with contaminated wetland soil. Resour. Conserv. Recycl. 140, 278–285.
- Yi, H., Yan, M., Huang, D., Zeng, G., Lai, C., Li, M., Huo, X., Qin, L., Liu, S., Liu, X., 2019. Synergistic effect of artificial enzyme and 2D nano-structured Bi₂WO₆ for eco-friendly and efficient biomimetic photocatalysis. Appl. Catal. B: Environ. 250, 52–62.
- Yu, J., Feng, H., Tang, L., Pang, Y., Zeng, G., Lu, Y., Dong, H., Wang, J., Liu, Y., Feng, C., 2020. Metal-free carbon materials for persulfate-based advanced oxidation process: microstructure, property and tailoring. Prog. Mater. Sci. 111, 100654.
- Yuan, S., Wang, M., Liu, J., Guo, B., 2020. Recent advances of SBA-15-based composites as the heterogeneous catalysts in water decontamination: a mini-review. J. Environ. Manage. 254, 109787.
- Yuan, X., Duan, S., Wu, G., Sun, L., Cao, G., Li, D., Xu, H., Li, Q., Xia, D., 2018a. Enhanced catalytic ozonation performance of highly stabilized mesoporous ZnO doped g-C₃N₄ composite for efficient water decontamination. Appl. Catal. A: Gen. 551, 129–138.
- Yuan, X., Qin, W., Lei, X., Sun, L., Li, Q., Li, D., Xu, H., Xia, D., 2018b. Efficient enhancement of ozonation performance via ZVZ immobilized g-C₃N₄ towards superior oxidation of micropollutants. Chemosphere 205, 369–379.
- Yuan, X., Xie, R., Zhang, Q., Sun, L., Long, X., Xia, D., 2019. Oxygen functionalized graphitic carbon nitride as an efficient metal-free ozonation catalyst for atrazine removal: performance and mechanism. Sep. Purif. Technol. 211, 823–831.
- Yue, D., Qian, X., Kan, M., Fang, M., Jia, J., Yang, X., Zhao, Y., 2018. A metal-free visible light active photo-electro-Fenton-like cell for organic pollutants degradation. Appl. Catal. B: Environ. 229, 211–217.
- Zhang, C., Lai, C., Zeng, G., Huang, D., Yang, C., Wang, Y., Zhou, Y., Cheng, M., 2016. Efficacy of carbonaceous nanocomposites for sorbing ionizable antibiotic sulfamethazine from aqueous solution. Water Res. 95, 103–112.
- Zhang, C., Zhou, Y., Wang, W., Yang, Y., Zhou, C., Wang, L., Lei, L., He, D., Luo, H., Huang, D., 2020a. Formation of Mo₂C/hollow tubular g-C₃N₄ hybrids with favorable charge transfer channels for excellent visible-light-photocatalytic performance. Appl. Surf. Sci., 146757.
- Zhang, M., Yeoh, F., Du, Y., Lin, K.A., 2019a. Magnetic cobalt-embedded carbon nitride composite derived from one-dimensional coordination polymer as an efficient catalyst for activating oxone to degrade methyltheobromine in water. Sci. Total Environ. 678, 466–475.
- Zhang, R., Wang, X., Zhou, L., Liu, Z., Crump, D., 2018. The impact of dissolved oxygen on sulfate radical-induced oxidation of organic micro-pollutants: a theoretical study. Water Res. 135, 144–154.
- Zhang, X., Xie, X., Wang, H., Zhang, J., Pan, B.C., Xie, Y., 2013. Enhanced photoresponsive ultrathin graphitic-phase C₃N₄ nanosheets for bioimaging. J. Am. Chem. Soc. 135 (1), 18–21.
- Zhang, X., Zhao, R., Zhang, N., Su, Y., Liu, Z., Gao, R., Du, C., 2020b. Insight to unprecedented catalytic activity of double-nitrogen defective metal-free catalyst: key role of coal gangue. Appl. Catal. B: Environ. 263, 118316.
- Zhang, Y., Li, Q., Long, Y., Zou, J., Song, Z., Liu, C., Liu, L., Qi, F., Xu, B., Chen, Z., 2019b. Catalytic ozonation benefit from the enhancement of electron transfer by the coupling of g-C₃N₄ and LaCoO₃: discussion on catalyst fabrication and electron transfer pathway. Appl. Catal. B: Environ. 254, 569–579.
- Zhou, C., Zeng, G., Huang, D., Luo, Y., Cheng, M., Liu, Y., Xiong, W., Yang, Y., Song, B., Wang, W., 2020a. Distorted polymeric carbon nitride via carriers transfer bridges with superior photocatalytic activity for organic pollutants oxidation and hydrogen production under visible light. J. Hazard. Mater. 386, 121947.
- Zhou, C., Zeng, Z., Zeng, G., Huang, D., Xiao, R., Cheng, M., Zhang, C., Xiong, W., Lai, C., Yang, Y., 2019. Visible-light-driven photocatalytic degradation of sulfamethazine by surface engineering of carbon nitride: properties, degradation pathway and mechanisms. J. Hazard. Mater. 380, 120815.
- Zhou, X., Zeng, Z., Zeng, G., Lai, C., Xiao, R., Liu, S., Huang, D., Qin, L., Liu, X., Li, B., 2020b. Persulfate activation by swine bone char-derived hierarchical porous carbon: multiple mechanism system for organic pollutant degradation in aqueous media. Chem. Eng. J. 383, 123091.
- Zhu, C., Zhu, F., Liu, C., Chen, N., Zhou, D., Fang, G., Gao, J., 2018. Reductive hexachloroethane degradation by S₂O₈²⁻ with thermal activation of persulfate under anaerobic conditions. Environ. Sci. Technol. 52 (15), 8548–8557.
- Zhu, J., Zhu, X., Cheng, F., Li, P., Wang, F., Xiao, Y., Xiong, W., 2019. Preparing copper doped carbon nitride from melamine templated crystalline copper chloride for Fenton-like catalysis. Appl. Catal. B: Environ. 256, 117830.